Scilight

Plant Ecophysiology

www.sciltp.com/journals/PlantEcophys

Article

Check for updates

Experimental Evidence for Coordinated Leaf Trait Responses to Elevated CO_2 in Five Common Crop Species

Astrid Odé [1,*], Paul L. Drake [2], Erik J. Veneklaas [2,3], Jan A. Lankhorst [1], Karin T. Rebel [1] and Hugo J. de Boer [1]

[1] Environmental Sciences, Copernicus Institute of Sustainable Development, Utrecht University, 3584 CB Utrecht, The Netherlands
[2] School of Biological Sciences, University of Western Australia, Crawley, WA 6009, Australia
[3] Institute of Agriculture, The University of Western Australia, Crawley, WA6009, Australia
* Correspondence: a.ode@uu.nl

How To Cite: Odé A, Drake PL, Lankhorst JA, Rebel KT, & de Boer HJ. Experimental Evidence for Coordinated Leaf Trait Responses to Elevated CO_2 in Five Common Crop Species. *Plant Ecophysiology* **2026**, *2*(1), 3. https://doi.org/10.53941/plantecophys.2026.100003

Publication History

Received: 19 December 2025
Revised: 22 March 2026
Accepted: 9 April 2026
Published: 15 April 2026

Abstract: Understanding leaf trait responses to changing atmospheric CO_2 concentrations ($[CO_2]$) is essential for land- surface modelling. Eco-evolutionary optimality (*EEO*) theory predicts coordinated responses in leaf traits that maintain a balance of maximum carbon assimilation gain with minimal summed resource use costs. Although individual leaf trait responses to atmospheric $[CO_2]$ changes are relatively well understood, few experiments have documented coordination of responses across functional leaf trait categories related to photosynthesis, photosynthetic biochemistry, stomatal conductance (g_s), and morphology. We examined leaf trait coordination in five common crop species, including buckwheat (C_3), common bean (C_3), maize (C_4), soybean (C_3), and wheat (C_3). We specifically included traits relevant for testing *EEO* theory, including diurnal measurements of g_s. Our results showed that among the four C_3 species, g_s and photosynthetic biochemistry traits were generally downregulated under elevated atmospheric $[CO_2]$, while photosynthetic rates increased, in line with P-model predictions. A principal component analysis (*PCA*) on the response ratios across C_3 species revealed coordinated trait variation along two main axes: principal component (*PC*) 1 mainly described leaf economic traits and *PC2* was mainly related to photosynthetic biochemistry and hydraulic capacity, indicating partial decoupling of leaf trait coordination. Intraspecific variation can arise from differences in photosynthetic pathways, as shown by the distinctive responses of the C_4 species maize, with potential consequences for trait coordination. Our results provide support for *EEO* theory on predictions of leaf trait combinations and vegetation patterns under future climates.

Academic Editor

Louis Santiago

Keywords: eco-evolutionary optimality; leaf trait coordination; vegetation modelling; photosynthetic capacity; stomatal conductance; leaf economic spectrum

1. Introduction

Understanding vegetation responses to anthropogenically increased atmospheric CO_2 concentration ($[CO_2]$) is essential to accurately predict and interpret global water and carbon fluxes (Prentice & Cowling, 2013; Calvin et al., 2023). Global dynamic vegetation models (*GDVM*'s) combined with photosynthesis models can be used to predict changes in primary productivity (Prentice & Cowling, 2013; Prentice et al., 2015). A promising approach for understanding and simulating these vegetation responses is eco-evolutionary optimality (*EEO*) theory, which states that uncompetitive leaf trait combinations are filtered out over time by natural selection (Prentice et al., 2014; Franklin et al., 2020; Harrison et al., 2021; Mengoli et al., 2022). Community-mean leaf trait values, as used in an *EEO*-based model based on Prentice et al. (2014) and referred to as the P-model from here onwards, are a combination of both phenotypic plasticity and

Copyright: © 2026 by the authors. This is an open access article under the terms and conditions of the Creative Commons Attribution (CC BY) license (https://creativecommons.org/licenses/by/4.0/).
Publisher's Note: Scilight stays neutral with regard to jurisdictional claims in published maps and institutional affiliations.

evolutionary outcomes (Harrison et al., 2021), shaping population trait means to maintain a balance of maximum carbon assimilation gain with minimal summed resource use costs (Dong et al., 2020; Harrison et al., 2021).

Evolutionary processes act over time-scales of decades to millions of years, whereas on a shorter time-scale of leaf trait acclimation (weeks to years), phenotypic plasticity allows for additional trait variation within genotypes (Franks, Drake, & Beerling, 2009; Odé et al., 2025). The *EEO*-based P-model is based on the premise that plants optimize their ratio of leaf intercellular [CO_2] to atmospheric [CO_2], denoted the c_i:c_a ratio and also termed χ (for the definitions of the symbols used in this paper, see Table 1) (Prentice et al., 2014; Stocker et al., 2020).This is accomplished by adjusting a multitude of leaf functional traits that can be categorized in line with Odé et al. (2025) as those related to stomatal conductance (g_s), photosynthetic biochemistry, morphology, and the overarching category 'photosynthesis' which includes traits that integrate multiple underlying leaf traits from these categories (Odé et al., 2025). The P-model can predict these optimal trait combinations, including values of g_s, the maximum rate of carboxylation (V_{cmax}) and maximum rate of electron transport (J_{max}), χ, and nitrogen content, using only environmental variables including temperature, elevation, humidity, atmospheric [CO_2], and light quantity (Prentice et al., 2014; Stocker et al., 2020). These predictions then allow for evaluation by comparing measured trait values under ambient and elevated atmospheric [CO_2] with the P-model outputs, allowing the model to be tested and refined (Harrison et al., 2021).

Table 1. Table of symbols and their corresponding definition and units.

Symbol	Definition	Units
A_{max}	Maximum rate of CO_2-saturated photosynthesis	μmol m^{-2} s^{-1}
A_{sat}	Light-saturated photosynthesis rate	μmol m^{-2} s^{-1}
C:N ratio	Ratio of carbon to nitrogen per leaf area	Unitless
c_i:c_a	ratio of leaf intercellular CO_2 concentration to atmospheric CO_2 concentration	Unitless
g_s	Stomatal conductance	mol m^{-2} s^{-1}
$g_{s(avg)}$	Time-averaged diurnal stomatal conductance	mol m^{-2} s^{-1}
$g_{s(op)}$	Operational stomatal conductance	mol m^{-2} s^{-1}
$g_{s(P\text{-}model)}$	Optimal stomatal conductance as predicted by the P-model	mol m^{-2} s^{-1}
g_{smax}	Maximum anatomical stomatal conductance	mol m^{-2} s^{-1}
J_{1000}	Light saturated rate of electron transport	μmol m^{-2} s^{-1}
J_{max}	Maximum rate of electron transport	μmol m^{-2} s^{-1}
LMA	Leaf dry mass per area	g m^{-2}
N_{area}	Nitrogen per leaf area	g m^{-2}
V_{cmax}	Maximum rate of carboxylation	μmol m^{-2} s^{-1}
V_{pmax}	maximum activity of phosphoenolpyruvate carboxylase	μmol m^{-2} s^{-1}
χ	Optimal c_i:c_a ratio as predicted by the P-model	Unitless
χ_{iso}	Isotope-derived c_i:c_a ratio	Unitless

The P-model predicts that similar values of χ can be achieved with a range of different underlying trait combinations across functional trait categories, each imposing specific temporal and structural constraints on leaf-level adjustments within the limits of the phenotypic plasticity of a genotype (Prentice et al., 2014; Harrison et al., 2021; Odé et al., 2025). This range of combinations reflects how leaf traits vary in concert rather than individually, both within and across species, a phenomenon known as trait coordination (Wright et al., 2004; Maire et al., 2013; Siefert et al., 2015; Zhou, Cieraad, & van Bodegom, 2022; Wang et al., 2023). Trait coordination reflects underlying physiological constraints or trade-offs between traits to cope with varying environments (Wright et al., 2004; Sanchez-Martinez et al., 2020, 2024). For example, the trade-off between stomatal density versus stomatal size (Lammertsma et al., 2011; de Boer et al., 2016), and the positive relationship between photosynthetic rate and stomatal conductance in sun versus shade leaves, reflecting increased photosynthetic demands under high light (Wong, Cowan, & Farquhar, 1979). However, trait coordination can also arise due to shared environmental responses without a direct mechanistic link between traits, e.g., in case of concerted convergence (Givnish et al., 2005). Regardless of the underlying cause, understanding trait coordination is essential to validate and improve *EEO*-based modelling approaches (Deans et al., 2020; Harrison et al., 2021).

Previous research on C_3 species has established that elevated atmospheric [CO_2] increases net photosynthetic rates (Norby et al., 2005; Ainsworth & Long, 2005; Leakey et al., 2009; Schimel, Stephens, & Fisher, 2015) despite a downregulation in photosynthetic biochemistry traits (Long et al., 2004; Lee, Barrott, & Reich, 2011; Zheng et al., 2019; Wang et al., 2020). This is in line with P-model predictions, and in addition, *EEO*-theory combined with the coordination hypothesis (Maire et al., 2012; Harrison et al., 2021) also predicts that responses in the maximum rate of carboxylation (V_{cmax}) and maximum rate of electron transport (J_{max}) are balanced to prevent overinvestment in either trait (Wang et al., 2017). Leaf nitrogen content per leaf area (N_{area}) is often used to predict V_{cmax} (as nitrogen is the main component of ribulose bisphosphate carboxylase-oxygenase [Rubisco]) through parameterized relationships (Smith & Dukes, 2013), though research has shown this

relationship to be more complex and dynamically changing with environmental variability (Luo et al., 2021; Perkowski, Ezekannagha, & Smith, 2025).

Elevated atmospheric [CO_2] also generally reduces the operational stomatal conductance (g_s as it performs under natural field conditions, $g_{s(op)}$), ensuring optimal carbon gain with minimal water loss during the day, consistent with predictions from optimality-based stomatal theory and the P-model (Medlyn et al., 2011; Murray et al., 2020; Prentice et al., 2014). g_s is regulated by the stomatal pore size, which can operate through (energetically costly) changes in guard cell pressure within a range constrained by the anatomical maximum stomatal conductance (g_{smax}). g_{smax} is determined by cuticular morphology, specifically pore area, pore depth, and stomatal density. Despite this anatomical constraint, the stomatal pore size is highly dynamic on a short time scale (minutes to hours) and follows a predictable diurnal pattern which is tied to changes in environmental variables (mainly light and vapour pressure deficit, *VPD*) (Mcelwain, Yiotis, & Lawson, 2016; Matthews, Vialet-Chabrand, & Lawson, 2017). Taken together, the increase in atmospheric [CO_2] is predicted to decrease both V_{cmax} and g_s, while maintaining or increasing net photosynthesis rates, in line with predictions from the P-model.

Typically, g_s is measured at a single timepoint under midday conditions (*e.g.,* Murray et al., 2019). In the P-model, χ is optimized to ambient growth conditions in coordination with V_{cmax}, and a g_s that is coordinated with V_{cmax}, thus representing a time-averaged value ($g_{s(P\text{-}model)}$) (Stocker et al., 2020). As these three traits can vary at different time scales and especially g_s has strong diurnal variability (Odé et al., 2025), it is unclear whether conventional methods to measure g_s at a midday time (Mcelwain, Yiotis, & Lawson, 2016) accurately represents the optimized $g_{s(P\text{-}model)}$. Therefore, we aimed to determine whether the commonly used midday measurement of g_s can serve as a proxy for $g_{s(P\text{-}model)}$, by comparing it to a diurnally time-averaged measure of g_s. Additionally, Mcelwain, Yiotis, & Lawson, 2016 and Murray et al. (2020) found the $g_{s(op)}$:g_{smax} ratio to be conservative at approximately 0.25, reflecting a g_s where small changes in guard cell pressure lead to relatively large changes in stomatal pore size and consequent g_s, and thus an operational state that can exert most stomatal control over rates of gas exchange (Franks et al., 2012). Previous studies show that in general, both g_s (Ainsworth & Long, 2005) and g_{smax} (Lammertsma et al., 2011) decline under elevated atmospheric [CO_2], although there are exceptions, and g_{smax} may take multiple seasons and/or generations to fully respond (Hincke et al., 2016). Although the $g_{s(op)}$:g_{smax} ratio is commonly used for paleo-climate reconstruction purposes on an evolutionary timescale (e.g., Franks & Beerling, 2009; McElwain & Steinthorsdottir, 2017), it is also highly relevant on a timescale over which phenotypic plasticity occurs. In many vegetation models, the timescale for acclimation through phenotypic plasticity is typically similar to the timesteps, and since g_{smax} defines the operational limit of g_s, this anatomical trait may constrain the timeframe for the acclimation of $g_{s(op)}$ (Franks et al., 2012; Odé et al., 2025). Therefore, we examined the responses of $g_{s(op)}$:g_{smax} to elevated atmospheric [CO_2] in this experiment.

Previous research on leaf trait coordination has focused on a selection of trait categories (Cui et al., 2020; Li et al., 2023), effects of environmental change other than atmospheric [CO_2] (Conesa et al., 2020; Dong et al., 2020; Xie, Wang, & Li, 2022; Xiong, Douthe, & Flexas, 2018; Xu et al., 2021b), or trait coordination within a single species or genotype (Augustine & McCulloh, 2024; Blackman et al., 2016). Here we aim to examine the coordination of trait responses to elevated [CO_2] across multiple functional categories among multiple species. We selected a variety of five fast-growing common crop species established in the literature to improve understanding of the effect of rising atmospheric [CO_2] levels on plant performance (Zheng et al., 2019; Ainsworth & Long, 2021). We applied a variation on the principal component analysis (*PCA*) method to specifically examine the coordination of trait responses, rather than raw trait values, to focus on trait coordination within phenotypic plasticity ranges (Sanchez-Martinez et al., 2020, 2024; Anderegg, 2023). We paid particular attention to the traits that are relevant for the P-model, including V_{cmax}, J_{max}, g_s, c_i:c_a and the ratio of $g_{s(op)}$:g_{smax}, and compared them with P-model predictions. Owing to the importance of $g_{s(op)}$ in the coordination of gas exchange, this study compares the common midday measurement as a proxy for $g_{s(op)}$ with diurnally time-averaged measurements of g_s.

2. Methodology

2.1. Experimental design

The experiment was conducted at the University of Western Australia plant growth facilities (31°59′04.2″ S 115°49′10.9″ E). Five common crop species, consisting of the C_3 species soybean (*Glycine max*, strain PI408105A from Salim et al. (2022)), common bean (*Phaseolus vulgaris*, 'borlotti', sold by Mr. Fothergills), common wheat (*Triticum aestivum*), and buckwheat (*Fagopyrum esculentum*, sold by myorganics) and the C_4 species maize (*Zea mays*, 'Sweet Corn Early Extra Sweet F1', sold by Mr. Fothergills). For each species and treatment combination, 3 to 5 seeds were planted in 1 litre pots with sterilized potting soil, and supplemented with common slow release fertilizer grains (5 g/L). After germination, the seedlings were thinned to one plant per pot. All plants were grown in walk-in climate controlled chambers in a staggered fashion over time with 1 to 2 week increments separating each new cohort. Plants of each species were grown at an ambient atmospheric [CO_2] of 400 ppm ('AC' treatment) and a high atmospheric [CO_2] of 1000 ppm ('HC' treatment). Each species-treatment consisted of 9 replicate plants, except for buckwheat and maize which comprised 8 replicate plants. This resulted in a total of 86 plants. Table 2 provides an overview of the experimental

species, species properties and number of replicates. Measurements of each population started when the first fully-grown leaf was available, and the different sets of measurements for each species were implemented over a short time period to limit age effects (typically within 1–2 weeks). Plants were re-randomised regularly.

2.2. Plant growth conditions

Chamber environmental conditions used a day-night cycle of 12 + 12 h, with the daytime conditions between 9:00 am and 9:00 pm. Daytime conditions were set at 30 degrees Celsius (°C) and LED lights provided a photosynthetic photon flux of 700 µmol m^{-2} s^{-1}. Nighttime conditions were set at 20 °C and 0 µmol m^{-2} s^{-1} photosynthetic photon flux. The temperature ramp from 20 °C to 30 °C took 40 min. Relative humidity (*RH*) was set not to drop below 40% to prevent excessive evaporation. See Table 3 for an overview of the growth chamber conditions. Plants were watered by hand in the germination phase and, after thinning, watered by an automated dripping system per pot. Growth chamber atmospheric [CO_2] was controlled to allow addition but not removal of atmospheric [CO_2].

Table 2. Experimental species, species properties and number of replicate individuals (N) per species and atmospheric [CO_2] treatment combination.

Species	Photo-Synthetic Pathway	Type	N AC (400 ppm)	N HC (1000 ppm)	Life Form	Growth Form
Buckwheat *(Fagopyrum esculentum)*	C_3	Eudicot	8	8	Annual	Forb
Common bean *(Phaseolus vulgaris)*	C_3	Eudicot	9	9	Annual	Forb
Soybean (*Glycine max)*	C_3	Eudicot	9	9	Annual	Forb
Wheat (*Triticum aestivum)*	C_3	Monocot	9	9	Annual	Grass
Maize (*Zea mays)*	C_4 (NADP-ME subtype)	Monocot	8	8	Annual	Grass

Table 3. Overview of growth chamber conditions during daylength, including the growth chamber setpoint and the mean and standard deviation (SD) of the measured values inside the growth chambers of temperature, light, atmospheric [CO_2] concentration, $^{13}C/^{12}C$ air isotope ratio, and relative humidity.

Chamber Variable	Setpoint	AC Chamber (mean ± SD)	HC Chamber (mean ± SD)
Temperature (°C)	30	29.7 ± 1.39	29.7 ± 1.40
Light (µmol s^{-1} m^{-2})	700	700.1 ± 5.29	700.5 ± 6.9
Atmospheric [CO_2] (ppm)	400 or 1000	404.8 ± 14.8	1000.1 ± 62.7
$\delta^{13}C_{air}$ (‰)	-	−12.59 ± 0.23	−25.14 ± 0.06
Relative humidity (%)	>40%	49.7 ± 5.5	60.35 ± 5.7

2.3. Leaf gas exchange measurements

Leaf gas exchange and photosynthesis measurements were done using a LI6400/XT portable photosynthesis system. Continuous diurnal time series of g_s to water vapour were measured for all species except buckwheat. The LI6400/XT settings were configured to mimic the growth chamber conditions: CO_2-sample at native atmospheric [CO_2] (400 ppm or 1000 ppm), photosynthetically active radiation (*PAR*) 0 µmol m^{-2} s^{-1} in the dark period and 700 µmol m^{-2} s^{-1} in the light period, flow 400 µmol s^{-1}, and leaf temperature at 20 °C in the dark period and 30 °C in the light period. For each species-treatment combination, the first healthy, fully expanded leaf was measured from each individual plant every 1 to 1.5 h. This included three individual plants for common bean and soybean, and four individual plants for maize and wheat. For all wheat gas exchange measurements, two non-overlapping leaves per plant of similar age were enclosed within the sample chamber of the photosynthesis system to ensure that the sample chamber completely filled. Measurements were performed approximately between 7:30 AM and 8:00 PM. The stomatal conductance of the diurnal timeframe was measured as a fast measurement. That is, the stomatal conductance was recorded before the leaf started adjusting to the environment of LI6400/XT sample chamber, even though the environmental variables of the chamber were equivalent to those of the growth room. This resulted in 27–40 datapoints per species-treatment combination per day. The time-averaged g_s ($g_{s(avg)}$) of a leaf was calculated using the 'trapz' function of the R package 'pracma', version 2.4.4 (Borchers, 2011), which computes the area under the diurnal curve using the trapezoidal rule, divided by the total diurnal measurement time.

As described for the diurnal measurements, $g_{s(op)}$ recorded between 1:30 PM and 4:00 PM was taken as a fast measurement on all species to avoid acclimation to the LI6400/XT chamber. Leaves that were fully expanded and of approximately the same leaf age were selected and marked for measurement. One leaf of each replicate plant

per species-treatment combination was measured. To minimize differences in g_s due to the specific time of day between the two treatments, we alternately measured two plants per treatment. The Licor settings were the same as for the diurnal measurements to mimic the growth room conditions. In addition, directly after the $g_{s(op)}$ measurements, and while keeping the leaf in the Li6400/XT sensor head, a light-saturated photosynthesis (A_{sat}) measurement was taken by increasing the light quantity to 1000 µmol m^{-2} s^{-1}. For all species except buckwheat, an additional A_{sat} measurement was taken at 400 ppm CO_2-sample settings on the HC population in order to compare the impact of biochemical adjustment on photosynthetic capacity.

The relationships between A_{sat} and the intercellular [CO_2] concentration (C_i), termed A-C_i response curves, were measured over an interval of 3–5 days per species on the same leaves as the $g_{s(op)}$ measurements using the same photosynthesis system as described above. A total of 5–6 curves per species and treatment were derived, except buckwheat in the AC treatment, from which four curves were derived due to time constraints. Settings of the photosynthesis system were as follows: *PAR* 1000 µmol m^{-2} s^{-1} (determined to be a saturating level based on light response curves), leaf temperature (T_{leaf}) 30 °C, *RH* 50–70%. A-Ci curves were obtained after g_s had achieved a steady-state under an atmospheric [CO_2] within the leaf chamber (C_a) equivalent to the growth room concentration (400 or 1000 ppm). A range of C_i was achieved by varying C_a in a stepped sequence (Table 4). The maximum rates of V_{cmax} (µmol m^{-2} s^{-1}) and the potential electron transport rate at saturating light intensity termed J_{1000} (µmol m^{-2} s^{-1}) (Buckley & Diaz-Espejo, 2015) were estimated from the obtained A-C_i curves using the 'fitaci' function of the 'plantecophys' R package version 1.4–6 (Duursma, 2015), which estimates the photosynthetic parameters based on the Farquhar, von Caemmerer, & Berry (1980) biochemical model of C_3 photosynthesis. The estimated parameters were standardized to 25 °C as by default. For wheat we used the bilinear fit method, and for buckwheat we adjusted the alpha parameter to 0.4 to obtain fits. The obtained parameters will be referenced as V_{cmax25} and J_{1000} throughout the rest of the paper.

Table 4. Overview of the gas exchange- and photosynthesis measurements with their corresponding LI6400/XT settings of light quantity (µmol m^{-2} s^{-1}), and atmospheric [CO_2] concentration (ppm). AC represents the ambient atmospheric [CO_2] treatment and HC the high atmospheric [CO_2] treatment.

Measurement	Measured Treatments	Light (µmol m^{-2} s^{-1})	Photosynthesis System [CO_2] Setting (ppm)
A_{sat_400}	AC	1000	400
A_{sat_400}	HC	1000	400
A_{sat_1000}	AC	1000	1000
$g_{s(op)}$	AC	700	Growth chamber [CO_2]
$g_{s(op)}$	HC	700	Growth chamber [CO_2]
g_s (diurnal)	AC	700	Growth chamber [CO_2]
g_s (diurnal)	HC	700	Growth chamber [CO_2]
A-C_i curve	AC C_3 species	1000	400–300–150–50–400–600–800–1200–1500–1800–2000
A-C_i curve	HC C_3 species	1000	1000–800–600–400–300–150–50–400–1000–1200–1500–1800–2000
A-C_i curve	AC C_4 species	1000	400–300–200–100–50–400–600–800–1000–1400–1700–2000
A-C_i curve	HC C_4 species	1000	1000–800–600–400–300–200–150–100–50–400–1000–1200–1500–2000

For the C_4 species maize, we based our method on Fan et al. (2025) and estimated the maximum activity of phosphoenolpyruvate (PEP) carboxylase (V_{pmax}), corresponding to V_{pmaxA} in (Fan et al., 2025), which is related to the initial slope of the A-C_i curve (C_i < 100 ppm) as follows:

$$A = V_p - R_m = \frac{C_i V_{pmax}}{C_i + K_p} - R_m \quad (1)$$

where A is the net [CO_2] assimilation rate (µmol CO_2 m^{-2} s^{-1}), V_p is the rate of PEP carboxylation (µmol CO_2] m^{-2} s^{-1}), K_p is the [CO_2] Michaelis-Menten constant (µ bar), and R_m is the daytime mitochondrial respiration in mesophyll cells, assumed half the daytime leaf mitochondrial respiration rate (µmol CO_2 m^{-2} s^{-1}). K_p was adjusted for T_{leaf} following Boyd, Gandin, & Cousins (2015):

$$K_p = K_{p25} \times e^{Ea(T_{leaf}-25)/(298.15R(T_{leaf}+273.15))} \quad (2)$$

where K_{p25} is the K_p measured at 25 °C, E_a is the activation energy of K_p, and R is the molar gas constant. R_{day} was adjusted for T_{leaf} as:

$$R_{day} = R_{day25} \times Q10^{\frac{T_{leaf}-25}{10}} \quad (3)$$

where $Q10$ is 2 (Huntingford et al., 2013), and R_{day} is set at 1.1 (Fan et al. (2022). Since it is difficult to distinguish the limiting factors at high C_i, a region of the C_4 A-C_i curve where (co-)limitation by Rubisco activity, ribulose-1,5-bisphosphate (RuBP) regeneration and/or PEP regeneration is possible, we estimated the rate of CO_2-saturated net photosynthesis (A_{max}) using the range of C_i. A_{max} is limited by both V_{cmax25} and J_{max25} and was estimated as:

$$\theta\,(A + Rday)^2 - (aCi + Amax)(A + Rday) + \alpha CiAmax = 0 \quad (4)$$

where θ is the curvature factor of the A-C_i curve, assumed to be 0.7 (unitless) (Sonawane et al., 2018; Von

Caemmerer, 2021), and α is the initial A-C_i curve slope (μmol [CO_2] m^{-2} s^{-1}).

An overview of the gas exchange- and photosynthesis measurements and the corresponding settings of the photosynthesis system can be found in Table 4.

2.4. Stomatal morphology

Leaf epidermal imprints were taken from each plant per species-treatment combination, from the same leaf as the $g_{s(op)}$ and A-C_i measurements, at the end of the measuring period. A thin layer of transparent nail varnish of approximately 5 × 5 mm was applied on both sides of the leaf because all species were amphistomatous, avoiding the mid vein and leaf edges. After ~15 min of drying, the varnish was peeled off with cellophane tape and mounted onto a microscopy slide. Wheat imprints were made of both leaves per plant that were used for the LI6400/XT measurements, and the results were averaged for the two leaves, per leaf side. Microscope photos were taken on a Leica DM6000 microscope. Stomatal density was measured in ImageJ version 1.53t (Schneider, Rasband, & Eliceiri, 2012) from an average of 5 fields of view at 100× or 200× magnification per leaf side per sample. Stomatal dimensions were measured at 400× magnification, as an average of three stomata measured per sample per leaf surface (amounting to 27 measurements per species-treatment combination per leaf surface). Theoretical maximum stomatal conductance was calculated following Franks and Farquhar (2001) as

$$g_{smax} = \frac{D_s \times a_{max} \frac{d_{H2O}}{w_v}}{d_p + \frac{\pi}{2}\sqrt{a_{max}/\pi}} \quad (5)$$

where d_{H2O} is the diffusivity of water vapour in air; w_v is the molar volume of air normalized to 25 °C; d_p is the stomatal pore depth, which was assumed equal to the guard cell width. The maximum pore size, a_{max}, is assumed to be an ellipse for the species with kidney shaped stomata (buckwheat, common bean, soybean) and was calculated as: $a_{max} = \pi \times (pore\ length)^2/8$. Maximum pore size for the species with dumbbell shaped stomata (wheat and maize) is assumed to be rectangle shaped; a_{max} was therefore calculated as: $a_{max} = \pi \times (pore\ length)^2/10$ (Franks et al., 2014; SI Table 2). g_{smax} was then calculated as the sum of the abaxial- and adaxial g_{smax}. The stomatal ratio was calculated as abaxial stomatal density/total stomatal density (abaxial + adaxial), following Muir (2019).

2.5. Leaf morphology and leaf carbon and nitrogen content

The leaf of each plant used for gas-exchange and photosynthesis measurements was cut at the leaf base and stored immediately in sealed bags with moist tissue paper to avoid shrinkage due to desiccation. The leaves were scanned with an Epson photo scanner as soon as possible after harvest, and the area was measured in ImageJ version 1.53t to determine the projected leaf area. Leaves were then oven dried at 60 °C for at least 48 h, and weighted to obtain the dry mass. Leaf mas per area (LMA) was then calculated per leaf of each plant as dry mass divided by leaf projected area in g m^{-2}. Leaves were then finely ground using a Retsch MM400 ball-mill grinder (Verder Scientific, Inc., Newtown, PA, USA) and prepared for stable carbon isotope- and carbon and nitrogen content analysis, as a combined measurement. From the ground material 1 mg was weighed and leaf carbon and nitrogen content (g g^{-1}) was measured using a Thermo Scientific™ Flash IRMS™ Elemental Analyser (Waltham, MA, USA). Leaf nitrogen per unit leaf area (N_{area}, gN m^{-2}) was calculated by multiplying leaf nitrogen content (N_{mass}; gN g^{-1}) with LMA (g m^{-2}). Methodology on the leaf carbon isotopes and isotope derived χ ($\chi_{(iso)}$) can be found in the Supplemental Information.

2.6. Statistical analyses and modelling

All statistical analyses were conducted in R version 4.2.3. Data were quality checked and for each trait a linear model was built to investigate the impact of species, (CO_2) treatment, and species-treatment interaction on each trait. The models were tested for outliers using a Bonferroni outlier test with the function 'outlierTest' of the 'car' package (version 3.1-3) (Fox, Weisberg, & Price, 2001). Normal distribution of data was checked visually by QQ-plots and tested by the base R Shapiro-Wilk normality test. Normality of residuals was addressed using residual plots and the 'check_normality' function from the R package 'performance' (version 0.14.0) (Lüdecke et al., 2021). Data were log-transformed if this resulted in better residual plots. Species, treatment, and their interaction effects on group means were tested using a two-way Type II ANOVA when ANOVA assumptions were met. If significant interaction effects were detected, a Type III ANOVA was used. If the ANOVA assumption of normal data distribution was violated, we used a Kruskal-Wallis test, and a Bonferroni adjusted Dunn's test as post-hoc using the 'dunnTest' function from the R package 'FSA', version 0.10.0. If variances were unequally distributed, we used a Welch T-Test. Eta-squared (partial) effect sizes for ANOVA were calculated using the function 'etaSquared' from the R package 'lsr', version 0.5.2. The R package 'emmeans' version 1.11.0 (Lenth, 2017) was used for ANOVA post-hoc comparisons. Statistics for the photosynthetic biochemistry traits were done separately for the C_3 and C_4 species maize, due to their inherently different mechanisms for carbon fixation. Detailed statistical output can be found in Table S1.

For the response ratios, we calculated the average value for each trait across all C_3 species. The trait 'c_i:c_a ratio' is derived from measurements coincident with the A_{sat} measurement. Then the response ratio was calculated as

mean HC/mean AC and $\log_{10}$ transformed, where the standard error was obtained as the standard deviation of the response ratios across species divided by the square root of the number of species. A principal component analysis (*PCA*) and its visualisation using the function 'fviz_pca' from the R package 'factoextra' was applied (Kassambara & Mundt, 2016) on the $\log_{10}$ response ratios. For the *PCA* we selected only the C_3 species, since the C_4 species maize lacks data for the traits $\chi_{(iso)}$, V_{cmax25}, and J_{1000}, which we considered essential to the P-model. The *PCA* analysis was based on a selection of key trait responses per functional category, to avoid correlation due to underlying mathematical similarities (*e.g.,* we avoided using *LMA* and N_{area} together, since we used *LMA* as conversion factor for N_{area}). Since the *PCA* included fewer variables than leaf traits (one response ratio value for each leaf trait per species) and there is a limited sample size of four (C_3) species, we emphasize that this analysis was solely for trait relationship exploration and not for quantitative analysis and interpretation. Predictions from the P-model were obtained using an R implementation of the P-model as described by Smith et al. (2019), which is available on Github with DOI https://doi.org/10.5281/zenodo.14186765 (Nick Smith's Ecophysiology Lab, McNellis, & Keenan, 2024). This function will calculate optimal V_{cmax}, g_s, χ, and N_{area} from environmental input variables of temperature, *PAR*, *VPD*, elevation, and an estimate for the quantum efficiency of photosynthetic electron transport, and the curvature of the light response curve of photosynthetic electron transport. Environmental variables used as input corresponded to the growth chamber conditions (Table 3). Optimal A_{sat} was derived with the 'Photosyn' function of the 'plantecophys' R package version 1.4-6 (Duursma 2015) using the modelled optimal values of V_{cmax25}, $g_{s(p\text{-}model)}$ and saturating light level (1000 μmol s^{-1} m^{-2}) as input. The response ratios of the optimal trait predictions were then calculated similar to the mean measured traits ($\log_{10}$ (HC/AC)). Simulated c_i:c_a values were calculated using the same 'Photosyn' function, based on the measured V_{cmax25} and either $g_{s(op)}$ or $g_{s(avg)}$ values, with the growth chamber conditions provided as environmental input. For samples without V_{cmax25} measurement (but $g_{s(op)}$ and $g_{s(avg)}$ present) the average V_{cmax25} value of the corresponding species-treatment combination was used.

3. Results

3.1. Photosynthesis

The light-saturated photosynthetic rate (A_{sat}) was higher under elevated atmospheric [CO_2] in all species except wheat (Figure 1, A_{sat} (g400-m400) versus A_{sat} (g1000-m1000)). In the HC treatment, values of A_{sat} were higher by 36.9% ($p < 0.05$) in common bean, 43.7% ($p < 0.01$) in buckwheat, 69.0% ($p < 0.001$) in maize, and 64.3% ($p < 0.001$) soybean, respectively, while there was no treatment effect in wheat (2.29% lower). Overall, there was a significant species-treatment interaction between those populations ($p < 0.01$, $\eta^2 = 0.21$). Comparing A_{sat} (g400-m400) versus A_{sat} (g1000-m400) also revealed a significant interaction effect of species and treatment ($p < 0.05$, $\eta^2 = 0.16$). In this case, A_{sat} (g1000-m400) was lower than A_{sat} (g400-m400) in common bean by 74.3% ($p < 0.001$), in maize by 26.9% ($p < 0.05$), in soybean by 50.7% ($p < 0.01$), and in wheat by 52.2% ($p < 0.001$). The lower A_{sat} (g1000-m400) compared A_{sat} (g1000-m1000) reflects a stomatal response to atmospheric [CO_2] levels, since both populations were grown at the same [CO_2] but measured at different [CO_2] concentrations. The higher A_{sat} (g400-m400) versus A_{sat} (g1000-m400) may indicate a combination of a downregulation of photosynthetic biochemical capacity and a stomatal response to elevated atmospheric [CO_2].

$\delta^{13}C$ measurements were conducted, but the air in the HC chamber had an unusually low $\delta^{13}C$ composition, which resulted in calculated χ_{iso} values exceeding 1. Because c_i:c_a values above 1 are biologically difficult to explain and reliability was too uncertain (Figure S1), χ_{iso} values are not reported and not included in further analyses.

3.2. Photosynthetic biochemistry

V_{cmax25} of the C_3 species (Figure 2A) showed a significant species ($p < 0.001$, $\eta^2 = 0.79$) and treatment ($p < 0.001$, $\eta^2 = 0.33$) effect. At elevated atmospheric [CO_2], average V_{cmax25} was lower by 40.7% in common bean ($p < 0.001$), 5.87% in buckwheat (not significant, [NS]), 11.0% in soybean (NS) and 27.3% in wheat ($p < 0.05$). For J_{1000} (Figure 2B), there was a significant species effect in the C_3 species ($p < 0.001$, $\eta^2 = 0.67$), but no significant treatment effect. However, average J_{1000} was lower in HC compared to AC in common bean by 31.5% (NS), in soybean by 12.1% (NS), and in wheat by 2.37% (NS). In buckwheat, average J_{1000} was 1.71% (NS) higher in HC than in AC. Owing to the general downregulation of V_{cmax25} without significant treatment responses of J_{1000}, the ratio J_{1000}/V_{cmax25} (Figure 2C) shows a significant species ($p < 0.05$, $\eta^2 = 0.21$) and treatment ($p < 0.01$, $\eta^2 = 0.22$) effect within the C_3 species. Average values of the J_{1000}/V_{cmax25} ratio in HC were higher than AC in common bean by 16.5% ($p < 0.05$), in buckwheat by 10.8% (NS), in soybean by 0.274% (NS), and in wheat by 25.6% ($p < 0.05$). There was a significant species-treatment interaction effect on N_{area} ($p < 0.05$, $\eta^2 = 0.13$) (Figure 2D). Elevated atmospheric [CO_2] led to a lower average N_{area} in all species, specifically in common bean by 26.8% ($p < 0.05$), in buckwheat by 17.9% ($p < 0.001$), in soybean by 23.4% ($p < 0.001$), in wheat by 15.9% ($p < 0.05$), and in maize by 10.9% (NS). For the C_4 species maize, atmospheric [CO_2] had no significant treatment effect on V_{pmax}, as determined by a Welch T-Test, though average V_{pmax} was 14.6% higher at HC compared to AC (Figure 2E). There was also no significant treatment effect on A_{max}, as revealed by a T-Test, since average A_{max} was higher by only 2.88% in HC compared to AC (Figure 2F).

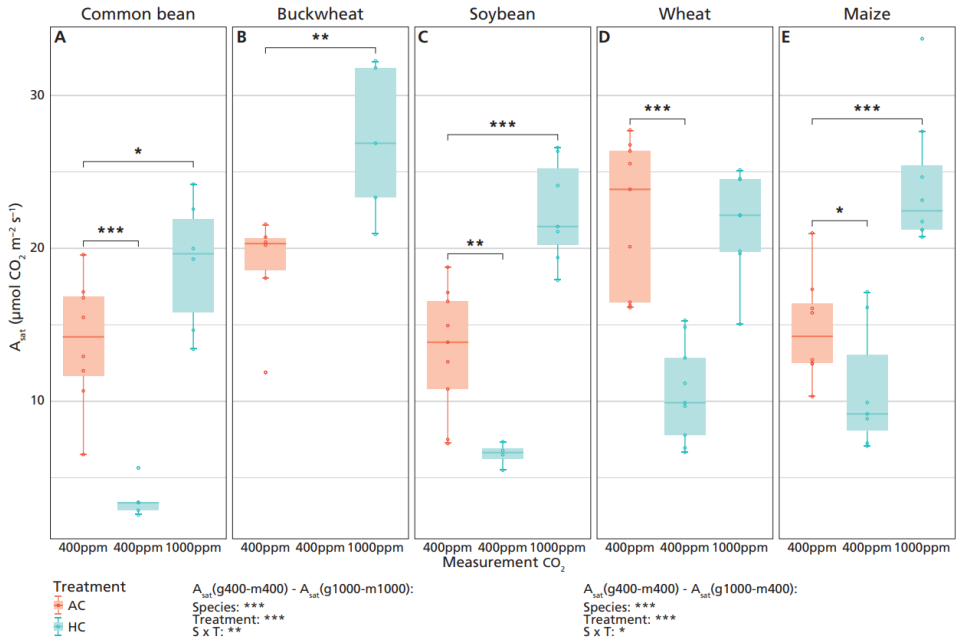

Figure 1. Boxplots of three different A_{sat} (µmol CO_2 m^{-2} s^{-1}) measurements per treatment and species. For each species, the AC population was measured at AC (400 ppm) CO_2 concentration (A_{sat} (g400-m400)), and the HC population was measured at HC (1000 ppm) CO_2 concentration (A_{sat} (g1000-m1000)) and AC (400 ppm) CO_2 concentration (A_{sat} (g1000-m400)). Point represent individual datapoints. Boxes indicate median, first quartile, and third quartile of the observed data. Whiskers are the furthest data point, no further than 1.5 times the inner quartile range. Species, treatment, and species x treatment interactions effects (S X T) significances are indicated as NS = not significant, * = $p < 0.05$, ** = $p < 0.01$, and *** = $p < 0.001$.

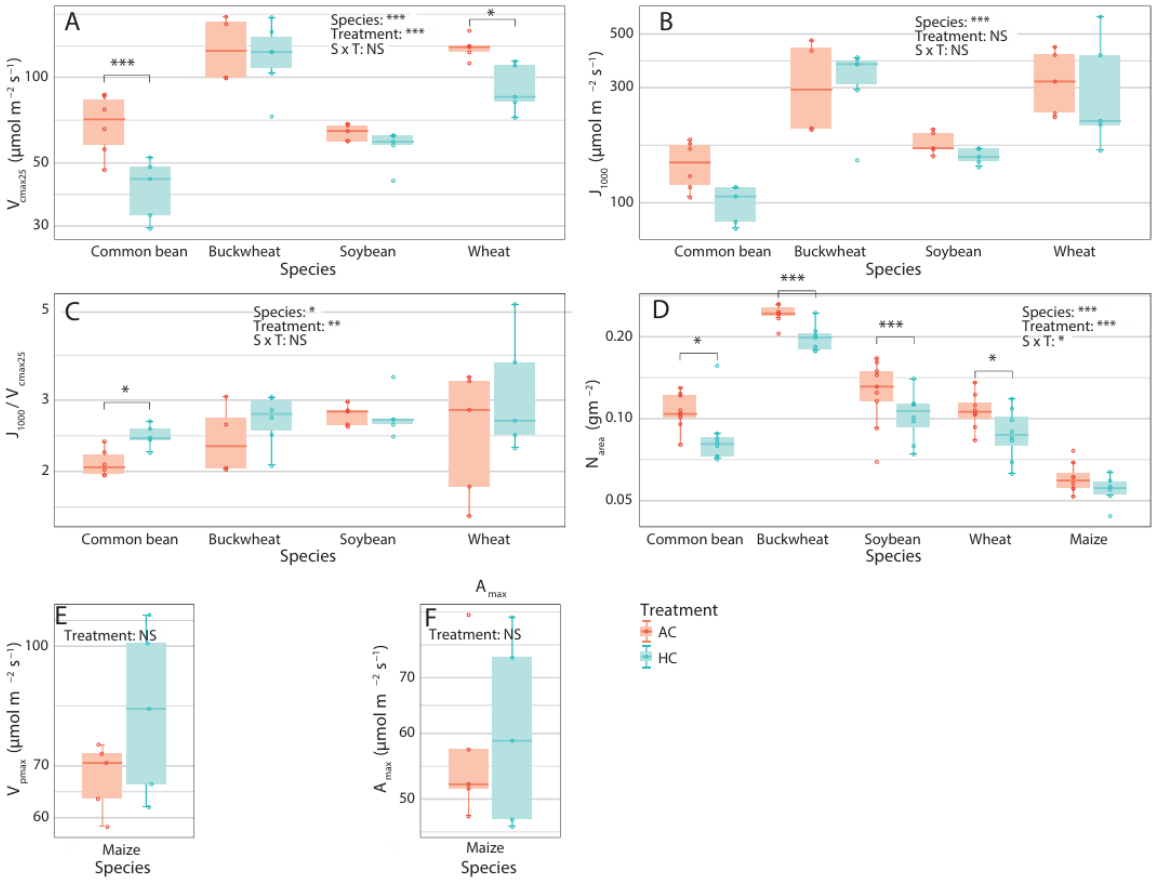

Figure 2. Boxplots of (**A**) V_{cmax25} (**B**) J_{1000} and (**C**) J_{1000}/V_{cmax25} of the C_3 species, ratio (**D**) N_{area} of all species, and (**E**) V_{pmax}, and (**F**) A_{max} of the C_4 species, per species and treatment. Boxes indicate median, first quartile, and third quartile of the observed data. Point represent individual datapoints. Values are plotted on a $\log_{10}$-transformed axis. Whiskers are the furthest data point, no further than 1.5 times the inner quartile range. Species, treatment, and species x treatment interactions effects (S X T) significances are indicated as NS = not significant, * = $p < 0.05$, ** = $p < 0.01$, and *** = $p < 0.001$.

3.3. Stomatal conductance

Diurnal measurements of g_s (Figure 3A–D) show large variability between species as well as within species. Values of g_s (mol m^{-2} s^{-1}) ranged between 0.0011–0.36 for common bean, 0.021–0.22 for maize, 0–0.40 for soybean, and 0–0.95 for wheat. There was a significant treatment effect on $g_{s(op)}$ ($p < 0.05$, $\eta^2 = 0.07$), besides an overall species effect on $g_{s(op)}$ ($p < 0.001$, $\eta^2 = 0.75$) (Figure 3E). The partial effect sizes imply that species is the main factor contributing to the variance in $g_{s(op)}$. Average values of $g_{s(op)}$ were lower under elevated atmospheric [CO_2] by 3.53% in common bean (NS), 1.96% in buckwheat (NS), 42.2% in maize ($p < 0.01$), and 32.4% (NS) in soybean. In contrast, in wheat $g_{s(op)}$ was higher by 20.0% (NS). The AC chamber's somewhat higher *VPD* could have reduced daytime stomatal opening, limiting the CO_2 treatment effects on $g_{s(op)}$. A significant species-treatment interaction effect on $g_{s(avg)}$ ($p < 0.05$, $\eta^2 = 0.38$) was found: under elevated [CO_2], average $g_{s(avg)}$ was higher by 43.2% (NS) in common bean and by 96.3% in wheat ($p < 0.01$), and decreased by 24.8% (NS) in maize, and 16.1% (NS) in soybean.

Elevated atmospheric [CO_2] had no significant treatment effect on g_{smax}, but variation in g_{smax} was mainly determined by species ($p < 0.001$) as revealed by a Kruskall-Wallis test (Figure 4A). Within species, Bonferroni-adjusted Dunn's Test showed that under elevated atmospheric [CO_2] average g_{smax} was lower in common bean by 15.1% (p.adjusted < 0.01), in buckwheat by 3.29% (NS), and in maize by 16.7% (p. adjusted < 0.05). In soybean, average g_{smax} increased by 16.8% (p.adjusted < 0.05) and in wheat by 1.22% (NS) under elevated atmospheric [CO_2]. There was a significant interaction effect between species and treatment (p <0.01, $\eta^2 = 0.16$) on the stomatal ratio (Figure 4B). The average stomatal ratio was lower under elevated atmospheric [CO_2] in common bean by 1.00% (NS), in maize by 9.95% ($p < 0.01$), in wheat by -0.227% (NS) and higher in soybean by 5.90% (NS) and in buckwheat by 3.62% (NS).

A significant species effect was found on both $g_{s(op)}$:g_{smax} ($p < 0.001$, $\eta^2 = 0.88$) (Figure 4C) and $g_{s(avg)}$:g_{smax} ($p < 0.01$, $\eta^2 = 0.89$) (Figure 4D). Under elevated atmospheric [CO_2], average $g_{s(op)}$:g_{smax} was higher by 8.17% (NS) in common bean, 11.7% (NS) in buckwheat, 20.3% (NS) in wheat, and lower by 22.2% in maize (NS), and 36.8% (NS) in soybean. Average values of $g_{s(avg)}$:g_{smax} were higher under elevated atmospheric [CO_2] by 80.2% (NS) in common bean, and 86.3% ($p < 0.05$) in wheat, and lower by 11.1% (NS) in maize and 23.0% (NS) in soybean.

3.4. Morphology

There was a significant species effect ($p < 0.001$) on leaf size as shown by a Kruskal-Wallis test (Figure 5A). Within species, a Bonferroni-adjusted Dunn's Test showed that under elevated atmospheric [CO_2] average leaf size was larger of common bean by 11.0% (p.adjusted < 0.05), buckwheat by 32.9% (NS), and soybean by 26.1% (p.adjusted < 0.05), whereas in maize and wheat, average leaf size was smaller by 30.0% (p.adjusted < 0.05) and 0.414% (NS) respectively. There was no significant treatment effect across all species, as tested by a Kruskall-Wallis test (NS), though overall these results show a pattern of larger leaf size*s* in the C_3 species and a smaller leaf size in the C_4 species maize.

There was a significant species-treatment interaction effect of elevated atmospheric [CO_2] on *LMA* ($p < 0.001$, eta = 0.28), where average *LMA* under elevated atmospheric [CO_2] was lower in common bean by 14.9% (NS), in wheat by 8.27% (NS), and in maize by 29.0% ($p < 0.001$), and higher in buckwheat by 6.59% (NS) and in soybean by 12.1% ($p < 0.05$) (Figure 5B). There was also a significant species-treatment interaction effect ($p < 0.001$, $\eta^2 = 0.30$) on the carbon to nitrogen ratio (*C:N* ratio) (Figure 5C). Average *C:N* ratio of all C_3 species was higher under elevated atmospheric [CO_2], specifically in common bean by 18.5% ($p < 0.05$), in buckwheat by 30.8% ($p < 0.01$), in soybean by 43.8% ($p < 0.001$), and in wheat by 12.8% (NS). In contrast, maize average *C:N* ratio was lower under elevated [CO_2] by 17.6% ($p < 0.05$).

3.5. Coordination of trait responses

A summary of the average leaf trait responses across the species is shown in Figure 6A, including the species-specific mean values. Traits are coloured by their corresponding functional trait category. Maize is included in the response ratios but not in the colored mean trait response bar (only the C_3 species). P-model predictions are included in panel A, as well as a prediction whereby both growth chamber had similar humidity levels, to investigate potential additional humidity effects. Generally, all traits in the category photosynthesis were increased, while those related to photosynthetic biochemistry were decreased. Traits related to stomatal conductance showed only a marginal response and these were more species-specific, but show an overall tendency to decrease. Traits related to morphology show an increase in *C:N* ratio, corresponding to the decrease in N_{area}. The absence of a mean trait response can reflect opposing underlying species-specific responses, for example for *LMA*. Comparing modelled optimal values using the growth chamber humidity with those using the AC humidity for both rooms revealed only a minor effect on the predicted optimal values.

Figure 6B shows a *PCA* on the response ratios of the C_3 species on a selection of key traits, which are underlined in Figure 6A. Principal component (*PC*) 1 explains 51.4% of the total variation, and *PC2* explains 34.4%. The *PCA* shows a clear grouping of the key trait responses to changes in atmospheric [CO_2] across the trait categories over the two main axes. *PC1* revealed high loadings of traits related to leaf economics, with highest loadings for A_{sat} (0.41), *C:N* ratio (0.44), leaf size (0.31), V_{cmax25} (0.37), c_i:c_a (−0.35), $g_{s(op)}$ (−0.42), and *PC2* revealed grouping of traits related to photosynthetic biochemistry and g_{smax}, with highest loadings for V_{cmax25} (0.28), N_{area} (0.55), J_{1000} (0.51), and g_{smax} (0.40).

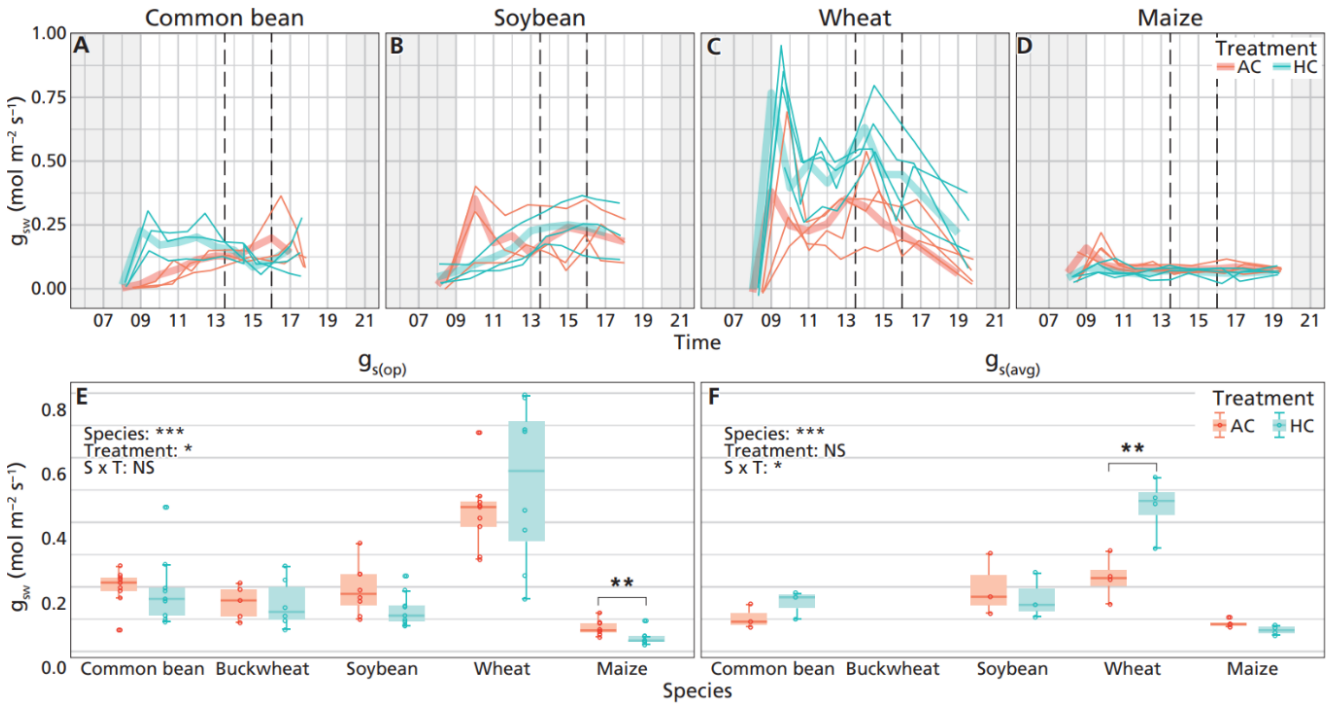

Figure 3. (**A**–**D**) Diurnal stomatal conductance over time per species and treatment. Each thin line corresponds to one leaf measured over one day, bold lines represent averages per treatment. Dark shaded zones represents the dark-period when lights were off (9:00 AM-9:00 PM). The dashed vertical lines represent the time-frame in which the $g_{s(op)}$ midday measurements were performed between 01:30–04:00 PM. Note that the datapoints of diurnal g_s and $g_{s(op)}$ are separate measurements. (**E**) Boxplots of stomatal conductance measured as midday $g_{s(op)}$ per species and treatment (**F**) Boxplots of g_s measured as $g_{s(avg)}$, calculated from the diurnal trajectories in panel (**A**–**D**). Boxes indicate median, first quartile, and third quartile of the observed data. Points in the boxes represent individual datapoints. Whiskers are the furthest data point, no further than 1.5 times the inner quartile range. Species, treatment, and species x treatment interactions effects (S X T) significances are indicated as NS = not significant, * = $p < 0.05$, ** = $p < 0.01$, and *** = $p < 0.001$.

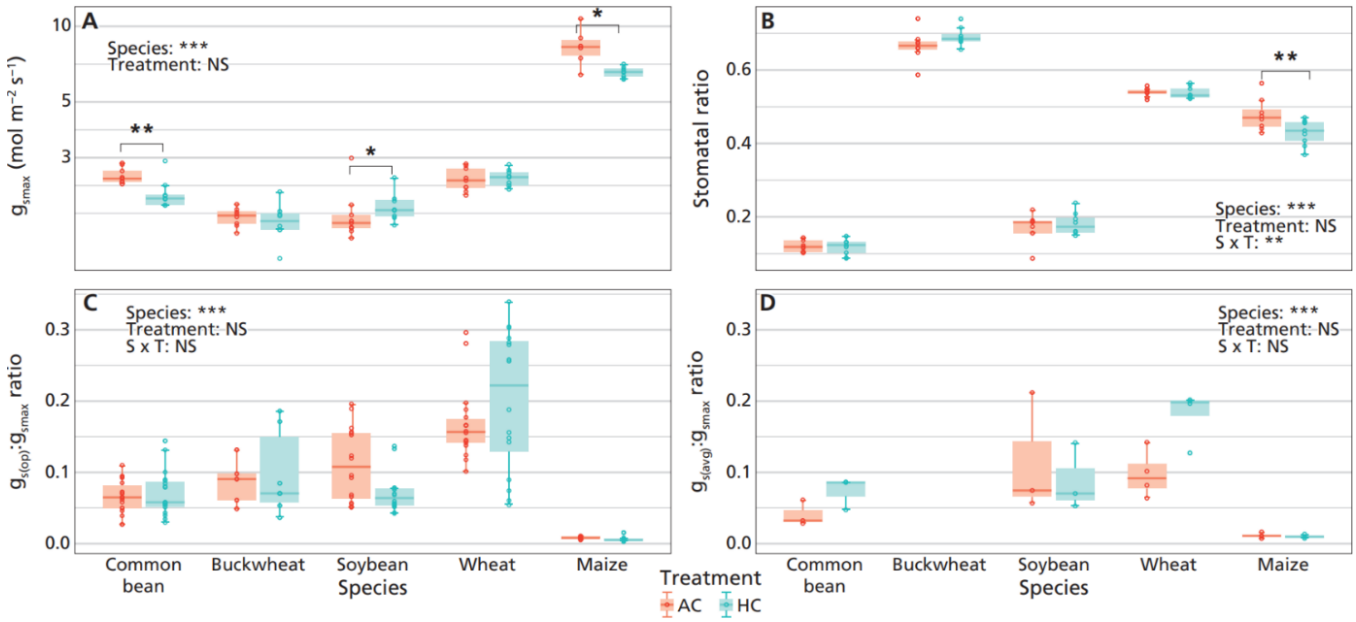

Figure 4. Boxplots of (**A**) g_{smax} (plotted on a $\log_{10}$-transformed axis) (**B**) Stomatal ratio (adaxial:total) (**C**) $g_{s(op)}$:g_{smax} ratio and (**D**) $g_{s(avg)}$:g_{smax} ratio, per species and treatment. Boxes indicate median, first quartile, and third quartile of the observed data. Points in the boxes represent individual datapoints. Whiskers are the furthest data point, no further than 1.5 times the inner quartile range. Species, treatment, and species x treatment interactions effects (S X T) significances are indicated as NS = not significant, * = $p < 0.05$, ** = $p < 0.01$, and *** = $p < 0.001$.

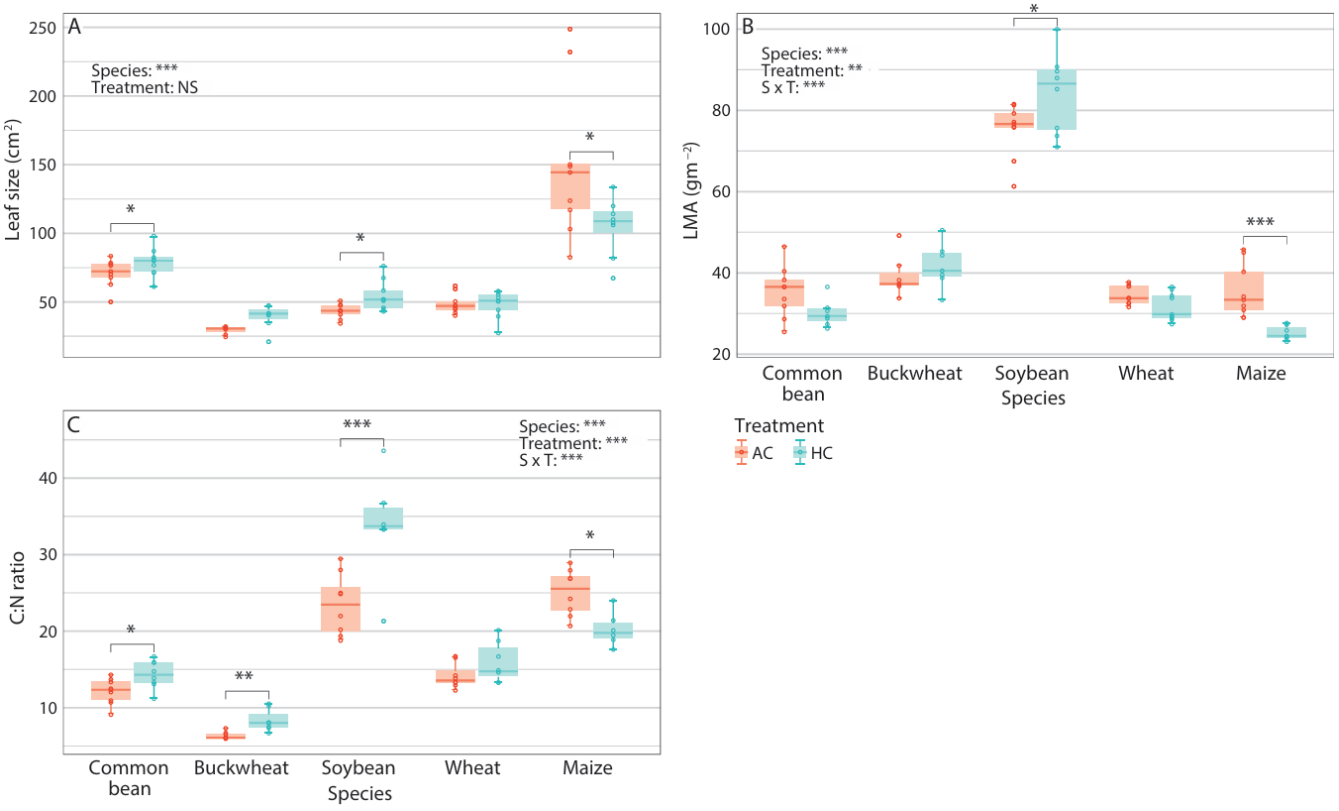

Figure 5. Boxplots of (**A**) leaf size, (**B**) LMA, and (**C**) C:N ratio, per species and treatment. Boxes indicate median, first quartile, and third quartile of the observed data. Points in the boxes represent individual datapoints. Whiskers are the furthest data point, no further than 1.5 times the inner quartile range. Species, treatment, and species x treatment interactions effects (S X T) significances are indicated as NS = not significant, * = $p < 0.05$, ** = $p < 0.01$, and *** = $p < 0.001$.

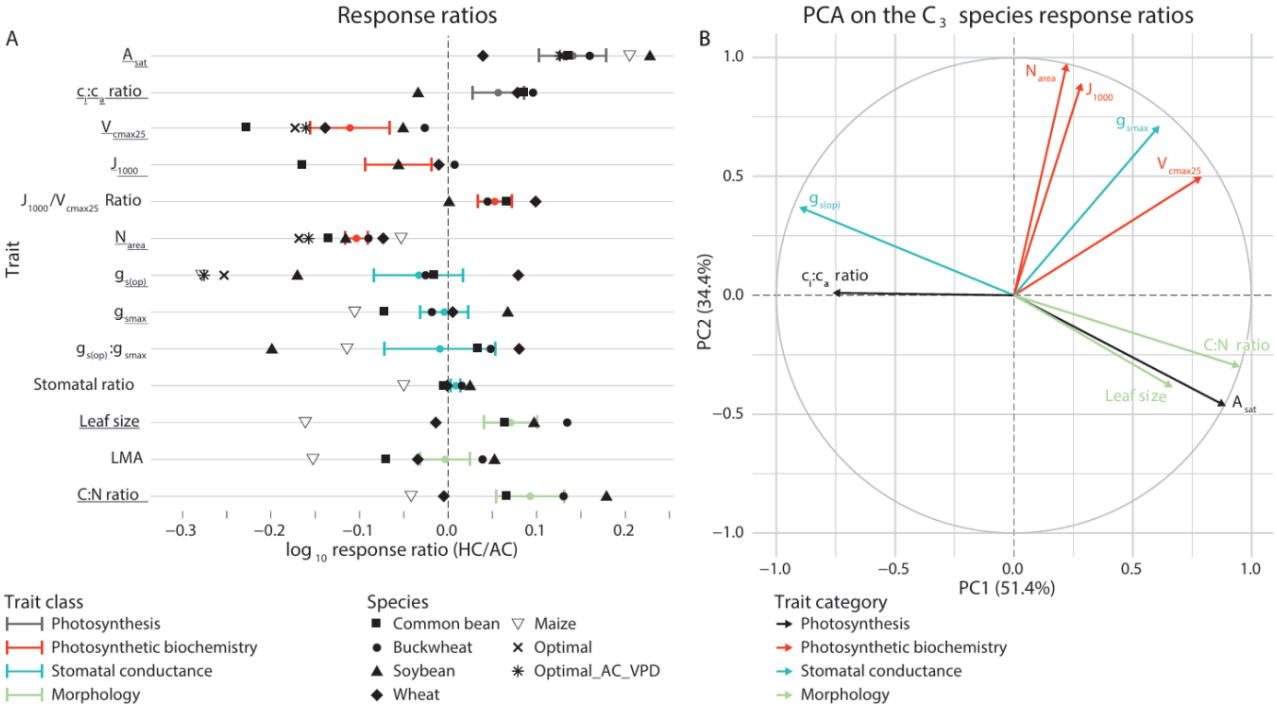

Figure 6. (**A**) Mean [CO_2] response ratios of leaf traits per species. Predicted optimal values of applicable traits are represented by the datapoints "Optimal", and a prediction whereby both growth chamber had similar humidity levels is indicated by "Optimal_AC_VPD". Data on the dashed 0-line means no mean response, negative values mean a decrease in the mean trait value and positive values mean an increase in the mean trait value. Colored bars indicate mean values (dot) with standard error (error bars) across the four C_3 species. Species-averages per trait are indicated by the individual datapoints. (**B**) PCA analysis on the response ratios across the C_3 species, so on the values of panel **A**. The x-axis is PC1 and the y-axis is PC2. Arrows are eigenvectors per trait values with their corresponding loading and direction. Colours represent the functional trait categories as structured throughout the results and panel **A**.

4. Discussion

The mean responses of leaf traits to elevated atmospheric [CO_2] across the C_3 species are in line with *EEO* theory and previous findings from atmospheric [CO_2] studies: traits related to photosynthetic biochemistry, as well as those associated with stomatal conductance, were generally downregulated, while photosynthetic rates were maintained or increased (Sage, Sharkey, & Seemann, 1989; Long et al., 2004; Ainsworth & Rogers, 2007; Leakey et al., 2009; Smith et al., 2019; Poorter et al., 2022). Under elevated atmospheric [CO_2], V_{cmax25} was downregulated more than J_{1000}, resulting in an increased J_{1000}/V_{cmax25} ratio. Together with the decrease in N_{area}, this is consistent with *EEO* theory and the coordination hypothesis, which propose that plants operate near the transition point between V_{cmax} and J_{max}, thereby optimizing leaf nitrogen allocation to photosynthetic capacity while avoiding overinvestment in V_{cmax}. (Maire et al., 2012; Smith & Keenan, 2020; Harrison et al., 2021; Dong et al., 2022; Perkowski, Ezekannagha, & Smith, 2025). The decrease in N_{area} observed in plants at elevated atmospheric [CO_2] could, in part, be attributed to a dilution effect by secondary compound accumulation (Poorter et al., 1997; Zheng et al., 2019). The increase in leaf size under elevated [CO_2] is in line with previous research, e.g., Pritchard et al. (1999), Ferris et al. (2001), Li, Kang, & Zhang (2004), and Poorter et al. (2022).

Values of g_s measured as midday $g_{s(op)}$ versus $g_{s(avg)}$ yielded comparable results: response magnitudes and directions were generally similar, except in common bean, likely due to differences in measurement timing in the diurnal g_s time course, where the diurnal g_s course showed a steep slope during the $g_{s(op)}$ measurement interval under AC but not HC. Differences in the diurnal g_s course between species can result from differences in stomatal opening/closing speed, sensitivity to water stress, and/or (an)isohydric strategy (Drake, Froend, & Franks, 2013; Klein, 2014; Grossiord et al., 2020). The larger range observed in $g_{s(op)}$ compared to $g_{s(avg)}$, especially in wheat, probably reflects the smoothing effect of averaging g_s over time, which dampens extreme values. Simulated $c_i{:}c_a$ responses using the Farquhar photosynthesis model (Farquhar et al., 1980) based on chamber conditions with measured V_{cmax25}, and either $g_{s(op)}$ *or* $g_{s(avg)}$ (Figure S2) also yielded comparable results. This shows that $g_{s(op)}$ measured as the less time-consuming midday g_s is a suitable proxy for the time-averaged $g_{s(p\text{-}model)}$, and therefore P-model testing, for the species and protocols of this study. There was no significant treatment effect on g_{smax}, perhaps the duration of this experiment was too short, although the relationship between atmospheric [CO_2] and g_{smax} remains weak/inconsistent over experiments and is subject to interaction with other environmental variables (Tricker et al., 2005; Ainsworth & Rogers, 2007; Xu et al., 2016; Poorter, Pons, & Reichgelt, 2025). Since g_{smax} showed limited response to elevated atmospheric [CO_2], the ratios $g_{s(op)}{:}g_{smax}$ and $g_{s(avg)}{:}g_{smax}$ were mainly driven by the effects on $g_{s(op)}$ and $g_{s(avg)}$, but those were too marginal to result in significant treatment effects.

The directions of the response ratios are generally in line with the predicted optimal values, though the magnitudes of some traits are smaller than predicted. This is particularly the case for $g_{s(op)}$ and to a smaller extent for V_{cmax25}, and the related N_{area}. The response ratios of the mean trait values show clear overall patterns, whereas the species-level data also reveals species-specific response magnitudes and/or directions. *LMA* was expected to increase under elevated atmospheric CO_2 (Poorter et al., 2009, 2022), though the growth temperature could have counteracted this effect (Poorter et al., 2009), resulting in the limited average response of *LMA*. Species-specific sensitivities to atmospheric [CO_2] and temperature, and/or additionally, differences in total non-structural carbohydrates build-up (Ainsworth et al., 2002; Poorter et al., 2009; Blackman et al., 2016), could then explain differences in *LMA* response between the species. Wheat showed, in contrast to the other (non-grass) species, limited/opposite responses in $g_{s(op)}$, A_{sat}, leaf size, and *C:N* ratio under elevated atmospheric [CO_2]. This could possibly be influenced by the timing of measurements within their lifespan (Cardoso-Vilhena & Barnes, 2001; Chavan et al., 2019) and/or high temperatures (Purcell et al., 2018; Bokshi et al., 2022). Species-specific differences can also arise from traits being inherently more or less plastic (Dong et al., 2020; Harrison et al., 2021), which can also be influenced by crop breeding techniques (Nimmo et al., 2023).

The C_4 species maize was included in our experiment to represent the fundamentally different response to C_i compared to C_3 species. Maize showed no significant response in photosynthetic biochemistry traits to elevated atmospheric [CO_2], which is consistent with previous (field) studies on C_4 species (Leakey, 2009; Fan et al., 2025). There was however an increase in A_{sat} under elevated atmospheric [CO_2] in line with previous findings, possibly pointing to an indirect result of interaction between water availability with reduced g_s (Ghannoum et al., 2000; Ainsworth & Rogers, 2007). Maize showed little variability of g_s during the day, which is typical for C_4 species (Taylor et al., 2010; Ghannoum, Al-Salman, & Cano, 2025). The observed decrease in g_s under elevated atmospheric [CO_2] is also in line with previous experiments (*e.g.,* Wei et al. (2022)), although Wei et al. (2022) reported an increase in g_{smax}, while (Han et al., 2023) observed a reduction in stomatal density, in line with our findings (stomatal density data not shown). Leaf size, *C:N* ratio, and *LMA* were higher under elevated atmospheric [CO_2], meaning that leaves were smaller and thinner. A decreased *LMA* in C_4 species is in line with (Poorter et al., 2009), though sample sizes were limited in that study. Overall, the observed differences in

this experiment between the C_3 and C_4 species trait responses to elevated atmospheric [CO_2] highlights the importance of representing their distinct photosynthetic pathways in (*EEO*-based) vegetation modelling.

The *PCA* on the response ratios revealed coordination of leaf traits across multiple functional trait categories among the C_3 species. *PC1* mainly captured variation of traits related to leaf economics, including $g_{s(op)}$, c_i:c_a, *C:N* ratio, V_{cmax25}, leaf size and A_{sat}. This aligns with the worldwide leaf economics spectrum (*WLES*) (Wright et al., 2004) which describes plant strategies along a continuum from fast to slow resource turnover. While trait covariation can arise from both common environmental drivers and plant strategies, Zhou, Cieraad, & van Bodegom, 2022 found that *WLES* traits mainly reflect plant strategies. *PC2* mainly describes the coordination of the photosynthetic biochemistry traits (V_{cmax25}, J_{1000}, N_{area}) and g_{smax}. This coordination is in line with the relationship between photosynthetic- and hydraulic capacity as described by (Brodribb et al., 2007; Brodribb & Feild, 2010; Sack et al., 2013), linked by the coupling between photosynthetic capacity and water transport. As stated by Blackman et al. (2016), the *WLES* framework together with the coordination between photosynthetic capacity and leaf hydraulics suggests that traits covary along a single axis (Reich, 2014; Blackman et al., 2016). However, several studies found trait decoupling between leaf economic traits and leaf hydraulics among species, e.g., Li et al. (2015); Maréchaux et al. (2015); Xiong, Douthe, & Flexas (2018), or even within genotypes of one species (Blackman et al., 2016). We note however, that our hydraulic traits are limited to those related to the stomata, and do not include those related to water transport traits such as xylem- or vein properties. Nevertheless, in line with these findings, our *PCA* revealed distinct axes of response variation between leaf economic traits and photosynthetic biochemistry- with (stomatal) hydraulic traits. This is in line with the P-model, which predicts how environmental variables influence the balance among leaf traits. Flexibility in trait response relationships may enhance phenotypic plasticity and allow new trait combinations to optimize χ. Since our study comprised a limited number of species, our *PCA* should not be over-interpreted, and the inclusion of a broader range of *WLES* species could provide insights into how species-specific strategies relate to level of plasticity (Maire et al., 2013) and underlying trait response decoupling.

The *PCA* conducted on our experimental data showed that leaf traits respond in a coordinated manner across C_3 species, although intraspecific responses reveal species-specific patterns. These species-level deviations can weaken trait-environment relationships when they diverge from community-level trends (Blackman et al., 2016; Henn et al., 2018; Zhou, Cieraad, & van Bodegom, 2022; Shao et al., 2022; Anderegg, 2023). Nevertheless, they remain important because they shape species-specific trade-offs and may influence plasticity to environmental change (Maire et al., 2013). Whether intraspecific variation needs to be taken into account in vegetation models also depends on the spatial scale of the study (Albert et al., 2011). In *EEO*-based models, intraspecific variability is implicitly included as it contributes to trait community-means, while evolutionary adaptations over longer timescales, such as the distinction between C_3 and C_4 species or between broadleaf- and needleleaf species, should be considered explicitly as they impose distinct constraints on plasticity ranges and timescales of acclimation (Odé et al., 2025). Extending this research to include a broader range of species, as well as incorporating whole-plant traits, will further improve *EEO*-based models and deepen our understanding of the coordination between photosynthetic and (stomatal) hydraulic traits (Laughlin, 2014; Xu et al., 2021a, 2021b; Joshi et al., 2022). Performing a *PCA* on trait response ratios rather than trait means is a novel variation on using *PCA* to investigate inter-trait relationships, and we encourage implementation of this approach to better understand coordinated trait responses to environmental change. Our results show that leaf traits respond in a coordinated manner across the C_3 crop species in this study, providing empirical insights to improve *EEO*-based vegetation models and predictions of leaf-, community-, and ecosystem-scale responses to future climate change.

5. Conclusions

This study presents experimental evidence for coordination of leaf trait responses to elevated atmospheric [CO_2] across a range of functional trait categories related to photosynthesis, photosynthetic biochemistry, morphology, and stomatal conductance. Across the C_3 species, trait responses were generally in line with predictions from *EEO*-theory and the *EEO*-based P-model. A novel variation of *PCA* analysis on the response ratios revealed coordination of trait acclimation to elevated atmospheric [CO_2], despite species-specific patterns. Intraspecific variation can arise from differences in species-specific strategies, or potentially from differences in photosynthetic pathway, as indicated by the distinctive responses of the C_4 species maize. Across the C_3 species a partial decoupling of leaf trait coordination was demonstrated by two main axes, capturing leaf economic traits, and photosynthetic biochemistry combined with hydraulic capacity. Providing experimental evidence of trait response coordination across C_3 species to elevated atmospheric [CO_2] improves our understanding of trait coordination across scales and contributes to refining *EEO*-based modelling approaches under future climate scenarios.

Supplementary Materials

The additional data and information can be downloaded at: https://media.sciltp.com/articles/others/2604130913254069/PlantEcophys-25120152-SM.pdf. References marked with an asterisk indicate studies included in the supplemental materials.

Author Contributions

AO, EJV, HJdB, JAL, KTR, and PLD designed the study and methodology. AO, EJV, JAL, and PLD conducted the experiment. AO, HJdB, KTR, and PLD analyzed the data and AO wrote the initial manuscript draft. AO, EJV, HJdB, JAL, KTR, and PLD reviewed and edited further versions of the manuscript, and approved the final version. All authors have read and agreed to the published version of the manuscript.

Funding

This project is supported by Schmidt Sciences.

Data Availability Statement

Data to support the findings of this study are openly available on https://github.com/AstridOde/PlantEcophys_data (accessed on 22 March 2026).

Acknowledgments

We thank Ton Markus for assistance with the figures. We thank two anonymous reviewers for their helpful comments on earlier versions of this manuscript.

Conflicts of Interest

Given the role as Associate Editor, Erik Veneklaas had no involvement in the peer review of this paper and had no access to information regarding its peer-review process. Full responsibility for the editorial process of this paper was delegated to another editor of the journal.

Use of AI and AI-Assisted Technologies

During the preparation of this work, the authors used ChatGPT (OpenAI) to improve the clarity and grammar of the English language and to assist in refining the R code. After using this tool, the authors reviewed and edited the content as needed and take full responsibility for the content of the published article.

Peer Review Statement

Plant Ecophysiology acknowledges the valuable contributions of Florian Busch and one anonymous reviewer to the peer review of this manuscript.

References

Ainsworth EA, Davey PA, Bernacchi CJ, Dermody OC, Heaton EA, Moore DJ, Morgan PB, Naidu SL, Ra HSY, Zhu XG, Curtis PS, & Long SP. (2002). A meta-analysis of elevated [CO_2] effects on soybean (Glycine max) physiology, growth and yield. *Global Change Biology*, *8*(8), 695–709. https://doi.org/10.1046/j.1365-2486.2002.00498.x

Ainsworth EA, & Long SP. (2005). What have we learned from 15 years of free-air CO_2 enrichment (FACE)? A meta-analytic review of the responses of photosynthesis, canopy properties and plant production to rising CO_2. *New Phytologist,* 165(2), 351–372. https://doi.org/10.1111/j.1469-8137.2004.01224.x

Ainsworth EA, & Long SP. (2021). 30 years of free-air carbon dioxide enrichment (FACE): What have we learned about future crop productivity and its potential for adaptation? *Global Change Biology, 27*(1), 27–49. https://doi.org/10.1111/gcb.15375

Ainsworth EA, & Rogers A. (2007). The response of photosynthesis and stomatal conductance to rising [CO2]: Mechanisms and environmental interactions. *Plant, Cell and Environment*, *30*(3), 258–270. https://doi.org/10.1111/j.1365-3040.2007.01641.x

Albert CH, Grassein F, Schurr FM, Vieilledent G, & Violle C. (2011). When and how should intraspecific variability be considered in trait-based plant ecology? Perspectives *Plant Ecology, Evolution and Systematics*, *13*(3), 217–225. https://doi.org/10.1016/j.ppees.2011.04.003

Anderegg LDL. (2023). Why can't we predict traits from the environment? *New Phytologist*, 237(6), 1998–2004. https://doi.org/10.1111/nph.18586

Augustine SP, & McCulloh KA. (2024). Physiological trait coordination and variability across and within three Pinus species. *New Phytologist*, 244(2), 451–463. https://doi.org/10.1111/nph.19859

Blackman CJ, Aspinwall MJ, Resco de Dios V, Smith RA, & Tissue DT. (2016). Leaf photosynthetic, economics and hydraulic traits are decoupled among genotypes of a widespread species of eucalypt grown under ambient and elevated CO_2. *Functional Ecology*, *30*(9), 1491–1500. https://doi.org/10.1111/1365-2435.12661

Bokshi AI, Thistlethwaite RJ, Chaplin ED, Kirii E, Trethowan RM, & Tan DKY. (2022). Physiological traits for evaluating heat-tolerance of Australian spring wheat cultivars at elevated CO_2. *Journal of Agronomy and Crop Science*, *208*(2), 178–196. https://doi.org/10.1111/jac.12584

Borchers HW. (2011). pracma: Practical Numerical Math Functions. In *CRAN: Contributed Packages*. CRAN. https://doi.org/10.32614/CRAN.package.pracma

Boyd RA, Gandin A, & Cousins AB. (2015). Temperature responses of C4 photosynthesis: Biochemical analysis of Rubisco, phosphoenolpyruvate carboxylase, and carbonic anhydrase in Setaria viridis. *Plant Physiology*, *169*(3), 1850–1861. https://doi.org/10.1104/pp.15.00586

Brodribb TJ, & Feild TS. (2010). Leaf hydraulic evolution led a surge in leaf photosynthetic capacity during early angiosperm diversification. *Ecology Letters*, *13*(2), 175–183. https://doi.org/10.1111/j.1461-0248.2009.01410.x

Brodribb TJ, Feild TS, & Jordan GJ. (2007). Leaf maximum photosynthetic rate and venation are linked by hydraulics. *Plant Physiology*, *144*(4), 1890–1898. https://doi.org/10.1104/pp.107.101352

Buckley TN, & Diaz-Espejo A. (2015). Reporting estimates of maximum potential electron transport rate. *New Phytologist*, *205*(1), 14–17. Blackwell Publishing Ltd. https://doi.org/10.1111/nph.13018

Cardoso-Vilhena J, & Barnes J. (2001). Does nitrogen supply affect the response of wheat (Triticum aestivum cv. Hanno) to the combination of elevated CO_2 and O_3? *Journal of Experimental Botany*, *52*(362), 1901–1911.

Chavan SG, Duursma RA, Tausz M, & Ghannoum O. (2019). Elevated CO_2 alleviates the negative impact of heat stress on wheat physiology but not on grain yield. *Journal of Experimental Botany*, *70*(21), 6447–6459. https://doi.org/10.1093/jxb/erz386

Conesa MA, Muir CD, Molins A, & Galmés J. (2020). Stomatal anatomy coordinates leaf size with Rubisco kinetics in the Balearic Limonium. *AoB PLANTS*, *12*(1), plz050. https://doi.org/10.1093/aobpla/plz050

Cui E, Weng E, Yan E, & Xia J. (2020). Robust leaf trait relationships across species under global environmental changes. *Nature Communications*, *11*(1), 2999. https://doi.org/10.1038/s41467-020-16839-9

de Boer HJ, Price CA, Wagner-Cremer F, Dekker SC, Franks PJ, & Veneklaas EJ. (2016). Optimal allocation of leaf epidermal area for gas exchange. *New Phytologist*, *210*(4), 1219–1228. https://doi.org/10.1111/nph.13929

Deans RM, Brodribb TJ, Busch FA, & Farquhar GD. (2020). Optimization can provide the fundamental link between leaf photosynthesis, gas exchange and water relations. *Nature Plants*, *6*(9), 1116–1125. https://doi.org/10.1038/s41477-020-00760-6

Dong N, Prentice IC, Wright IJ, Evans BJ, Togashi HF, Caddy-Retalic S, McInerney FA, Sparrow B, Leitch E, & Lowe AJ. (2020). Components of leaf-trait variation along environmental gradients. *New Phytologist*, *228*(1), 82–94. https://doi.org/10.1111/nph.16558

Dong N, Prentice IC, Wright IJ, Wang H, Atkin OK, Bloomfield KJ, Domingues TF, Gleason SM, Maire V, Onoda Y, Poorter H, & Smith NG. (2022). Leaf nitrogen from the perspective of optimal plant function. *Journal of Ecology*, *110*(11), 2585–2602. https://doi.org/10.1111/1365-2745.13967

Drake PL, Froend RH, & Franks PJ. (2013). Smaller, faster stomata: Scaling of stomatal size, rate of response, and stomatal conductance. *Journal of Experimental Botany*, *64*(2), 495–505. https://doi.org/10.1093/jxb/ers347

Duursma RA. (2015). Plantecophys—An R package for analysing and modelling leaf gas exchange data. *PLoS ONE*, *10*(11), e0143346. https://doi.org/10.1371/journal.pone.0143346

Fan Y, Asao S, Furbank RT, von Caemmerer S, Day DA, Tcherkez G, Sage TL, Sage RF, & Atkin OK. (2022). The crucial roles of mitochondria in supporting C4 photosynthesis. *New Phytologist*, *233*(3), 1083–1096. https://doi.org/10.1111/nph.17818

Fan Y, Noble DWA, Medlyn BE, Monson RK, Sage RF, Smith NG, Ainsworth EA, Busch FA, Danila FR, Ermakova M, Friesen P, Furbank RT, Gan SH, Ghannoum O, … & Way DA. (2025). Environmental factors have a greater influence on photosynthetic capacity in C4 plants than biochemical subtypes or growth forms. *New Phytologist*, *248*(3), 1205–1224. https://doi.org/10.1111/nph.70525

Farquhar GD, von Caemmerer S, & Berry JA. (1980). A biochemical model of photosynthetic CO_2 assimilation in leaves of C3 species. *Planta*, *149*(1), 78–90. https://doi.org/10.1007/BF00386231

*Farquhar GD, O'Leary MH, & Berry JA. (1982). On the relationship between carbon isotope discrimination and the intercellular carbon dioxide concentration in leaves. *Australian Journal of Plant Physiology*, *9*(2), 121–137. https://doi.org/10.1071/PP9820121

*Farquhar GD, & Richards RA. (1984). Isotopic composition of plant carbon correlates with water-use efficiency of wheat genotypes. *Australian Journal of Plant Physiology*, *11*(6), 539–552. https://doi.org/10.1071/PP9840539

*Feng X. (1999). Trends in intrinsic water-use efficiency of naural trees for the past 100-200 years: A response to atmospheric CO_2 concentration. *Geochimica et Cosmochimica Acta*, *63*(13–14), 1891–1903. https://doi.org/10.1016/S0016-7037(99)00088-5

Ferris R, Sabatti M, Miglietta F, Mills RF, & Taylor G. (2001). Leaf area is stimulated in Populus by free air CO2 enrichment (POPFACE), through increased cell expansion and production. *Plant, Cell and Environment*, *24*(3), 305–315. https://doi.org/10.1046/j.1365-3040.2001.00684.x

Fox J, Weisberg S, & Price B. (2001). car: Companion to Applied Regression. In *CRAN: Contributed Packages*. CRAN. https://doi.org/10.32614/CRAN.package.car

Franklin O, Harrison SP, Dewar R, Farrior CE, Brännström Å, Dieckmann U, Pietsch S, Falster D, Cramer W, Loreau M, Wang H, Mäkelä A, Rebel KT, Meron E, … & Colin I. (2020). Organizing principles for vegetation dynamics. *Nature Plants, 6*(5), 444–453. https://doi.org/10.1038/s41477-020-0655-x

Franks PJ, & Beerling DJ. (2009). Maximum leaf conductance driven by CO2 effects on stomatal size and density over geologic time. *Proceedings of the National Academy of Sciences of the United States of America*, *106*(25), 10343–10347. https://doi.org/10.1073/pnas.0904209106

Franks PJ, Drake PL, & Beerling DJ. (2009). Plasticity in maximum stomatal conductance constrained by negative correlation between stomatal size and density: An analysis using Eucalyptus globulus. *Plant, Cell and Environment*, *32*(12), 1737–1748. https://doi.org/10.1111/j.1365-3040.2009.002031.x

Franks PJ, & Farquhar GD. (2001). The Effect of Exogenous Abscisic Acid on Stomatal Development, Stomatal Mechanics, and Leaf Gas Exchange in Tradescantia virginiana. *Plant Physiology, 125*(2), 935–942.

Franks PJ, Leitch IJ, Ruszala EM, Hetherington AM, & Beerling DJ. (2012). Physiological framework for adaptation of stomata to CO_2 from glacial to future concentrations. *Philosophical Transactions of the Royal Society B: Biological Sciences*, *367*(1588), 537–546. https://doi.org/10.1098/rstb.2011.0270

Franks PJ, Royer DL, Beerling DJ, Van De Water PK, Cantrill DJ, Barbour MM, & Berry JA. (2014). New constraints on atmospheric CO_2 concentration for the Phanerozoic. *Geophysical Research Letters*, *41*(13), 4685–4694. https://doi.org/10.1002/2014GL060457

Ghannoum O, Al-Salman YM, & Cano FJ. (2025). Opportunities for improving intrinsic water use efficiency in C4 plants under climate change. *New Phytologist*, 248(6), 2656–2673. https://doi.org/10.1111/nph.70660

Ghannoum O, Von Caemmerer S, Ziska LH, & Conroy JP. (2000). The growth response of C4 plants to rising atmospheric CO2 partial pressure: A reassessment. *Plant, Cell and Environment*, *23*(9), 931–942. https://doi.org/10.1046/j.1365-3040.2000.00609.x

Givnish TJ, Pires JC, Graham SW, McPherson MA, Prince LM, Patterson TB, Rai HS, Roalson EH, Evans TM, Hahn WJ, Millam RC, Meerow AW, Molvray M, Kores PJ, … & Sytsma KJ. (2005). Repeated evolution of net venation and fleshy fruits among monocots in shaded habitats confirms a priori predictions: Evidence from an ndhF phylogeny. *Proceedings of the Royal Society B: Biological Sciences*, *272*(1571), 1481–1490. https://doi.org/10.1098/rspb.2005.3067

Grossiord C, Buckley TN, Cernusak LA, Novick KA, Poulter B, Siegwolf RTW, Sperry JS, & McDowell NG. (2020). Plant responses to rising vapor pressure deficit. *New Phytologist,* 226(6), 1550–1566. https://doi.org/10.1111/nph.16485

Han Y, Wang J, Zhang Y, & Wang S. (2023). Effects of Regulated Deficit Irrigation and Elevated CO2 Concentration on the Photosynthetic Parameters and Stomatal Morphology of Two Maize Cultivars. *Journal of Plant Growth Regulation*, *42*(5), 2884–2892. https://doi.org/10.1007/s00344-022-10754-7

Harrison SP, Cramer W, Franklin O, Prentice IC, Wang H, Brännström Å, de Boer H, Dieckmann U, Joshi J, Keenan TF, Lavergne A, Manzoni S, Mengoli G, Morfopoulos C, … & Wright IJ. (2021). Eco-evolutionary optimality as a means to improve vegetation and land-surface models. *New Phytologist*, *231*(6), 2125–2141. https://doi.org/10.1111/nph.17558

Henn JJ, Buzzard V, Enquist BJ, Halbritter AH, Klanderud K, Maitner BS, Michaletz ST, Pötsch C, Seltzer L, Telford RJ, Yang Y, Zhang L, & Vandvik V. (2018). Intraspecific trait variation and phenotypic plasticity mediate alpine plant species response to climate change. *Frontiers in Plant Science*, *9*, 1548. https://doi.org/10.3389/fpls.2018.01548

Hincke AJC, Broere T, Kürschner WM, Donders TH, & Wagner-Cremer F. (2016). Multi-year leaf-level response to sub-ambient and elevated experimental CO2 in Betula nana. *PLoS ONE*, *11*(6), e0157400. https://doi.org/10.1371/journal.pone.0157400

Huntingford C, Zelazowski P, Galbraith D, Mercado LM, Sitch S, Fisher R, Lomas M, Walker AP, Jones CD, Booth BBB, Malhi Y, Hemming D, Kay G, Good P, … & Cox PM. (2013). Simulated resilience of tropical rainforests to CO2-induced climate change. *Nature Geoscience*, *6*(4), 268–273. https://doi.org/10.1038/ngeo1741

IPCC. (2023). Climate Change 2023: Synthesis Report. In *Contribution of Working Groups I, II and III to the Sixth Assessment Report of the Intergovernmental Panel on Climate Change* (Lee H, Romero J. Eds.; 184p). IPCC. https://doi.org/10.59327/IPCC/AR6-9789291691647

Joshi J, Stocker BD, Hofhansl F, Zhou S, Dieckmann U, & Prentice IC. (2022). Towards a unified theory of plant photosynthesis and hydraulics. *Nature Plants*, *8*(11), 1304–1316. https://doi.org/10.1038/s41477-022-01244-5

Kassambara A, & Mundt F. (2016). factoextra: Extract and Visualize the Results of Multivariate Data Analyses. In *CRAN: Contributed Packages*. CRAN. https://doi.org/10.32614/CRAN.package.factoextra

Klein T. (2014). The variability of stomatal sensitivity to leaf water potential across tree species indicates a continuum between isohydric and anisohydric behaviours. *Functional Ecology*, *28*(6), 1313–1320. https://doi.org/10.1111/1365-2435.12289

Lammertsma EI, De Boer HJ, Dekker SC, Dilcher DL, Lotter AF, & Wagner-Cremer F. (2011). Global CO_2 rise leads to reduced maximum stomatal conductance in Florida vegetation. *Proceedings of the National Academy of Sciences of the United States of America*, *108*(10), 4035–4040. https://doi.org/10.1073/pnas.1100371108

Laughlin DC. (2014). The intrinsic dimensionality of plant traits and its relevance to community assembly. *Journal of Ecology*, *102*(1), 186–193. https://doi.org/10.1111/1365-2745.12187

Leakey ADB. (2009). Rising atmospheric carbon dioxide concentration and the future of C4 crops for food and fuel. *Proceedings of the Royal Society B: Biological Sciences 276*(1666), 2333–2343. https://doi.org/10.1098/rspb.2008.1517

Leakey ADB, Ainsworth EA, Bernacchi CJ, Rogers A, Long SP, & Ort DR. (2009). Elevated CO_2 effects on plant carbon, nitrogen, and water relations: Six important lessons from FACE. *Journal of Experimental Botany*, *60*(10), 2859–2876. https://doi.org/10.1093/jxb/erp096

Lee TD, Barrott SH, & Reich PB. (2011). Photosynthetic responses of 13 grassland species across 11 years of free-air CO_2 enrichment is modest, consistent and independent of N supply. *Global Change Biology*, *17*(9), 2893–2904. https://doi.org/10.1111/j.1365-2486.2011.02435.x

Lenth RV. (2017). emmeans: Estimated Marginal Means, aka Least-Squares Means. In *CRAN: Contributed Packages*. CRAN. https://doi.org/10.32614/CRAN.package.emmeans

Li F, He C, Chang Z, Ma C, Yu J, Liu L, Zhang Y, & Hao L. (2023). Effects of elevated carbon dioxide on plant growth and leaf photosynthesis of annual ryegrass along a phosphorus deficiency gradient. *Frontiers in Plant Science*, *14*. https://doi.org/10.3389/fpls.2023.1271262

Li F, Kang S, & Zhang J. (2004). Interactive effects of elevated CO_2, nitrogen and drought on leaf area, stomatal conductance, and evapotranspiration of wheat. *Agricultural Water Management*, *67*(3), 221–233. https://doi.org/10.1016/j.agwat.2004.01.005

Li L, McCormack ML, Ma C, Kong D, Zhang Q, Chen X, Zeng H, Niinemets Ü, & Guo D. (2015). Leaf economics and hydraulic traits are decoupled in five species-rich tropical-subtropical forests. *Ecology Letters*, *18*(9), 899–906. https://doi.org/10.1111/ele.12466

Long SP, Ainsworth EA, Rogers A, & Ort DR. (2004). Rising Atmospheric Carbon Dioxide: Plants FACE the future. *Annual Review of Plant Biology,* 55(1), 591–628. https://doi.org/10.1146/annurev.arplant.55.031903.141610

Luo X, Keenan TF, Chen JM, Croft H, Colin Prentice I, Smith NG, Walker AP, Wang H, Wang R, Xu C, & Zhang Y. (2021). Global variation in the fraction of leaf nitrogen allocated to photosynthesis. *Nature Communications*, *12*(1), 4866. https://doi.org/10.1038/s41467-021-25163-9

Maire V, Gross N, Hill D, Martin R, Wirth C, Wright IJ, & Soussana JF. (2013). Disentangling Coordination among Functional Traits Using an Individual-Centred Model: Impact on Plant Performance at Intra- and Inter-Specific Levels. *PLoS ONE*, 8(10), e77372. https://doi.org/10.1371/journal.pone.0077372

Maire V, Martre P, Kattge J, Gastal F, Esser G, Fontaine S, & Soussana JF. (2012). The coordination of leaf photosynthesis links C and N fluxes in C3 plant species. *PLoS ONE*, 7(6), e38345. https://doi.org/10.1371/journal.pone.0038345

Maréchaux I, Bartlett MK, Sack L, Baraloto C, Engel J, Joetzjer E, & Chave J. (2015). Drought tolerance as predicted by leaf water potential at turgor loss point varies strongly across species within an Amazonian forest. *Functional Ecology*, *29*(10), 1268–1277. https://doi.org/10.1111/1365-2435.12452

Matthews JSA, Vialet-Chabrand SRM, & Lawson T. (2017). Diurnal variation in gas exchange: The balance between carbon fixation and water loss. *Plant Physiology*, *174*(2), 614–623. https://doi.org/10.1104/pp.17.00152

McElwain JC, & Steinthorsdottir M. (2017). Paleoecology, ploidy, paleoatmospheric composition, and developmental biology: A review of the multiple uses of fossil stomata. *Plant Physiology 174*(2), 650–664. https://doi.org/10.1104/pp.17.00204

Mcelwain JC, Yiotis C, & Lawson T. (2016). Using modern plant trait relationships between observed and theoretical maximum stomatal conductance and vein density to examine patterns of plant macroevolution. *New Phytologist*, *209*(1), 94–103. https://doi.org/10.1111/nph.13579

Medlyn BE, Duursma RA, Eamus D, Ellsworth DS, Prentice IC, Barton CVM, Crous KY, De Angelis P, Freeman M, & Wingate L. (2011). Reconciling the optimal and empirical approaches to modelling stomatal conductance. *Global Change Biology*, *17*(6), 2134–2144. https://doi.org/10.1111/j.1365-2486.2010.02375.x

Mengoli G, Agustí-Panareda A, Boussetta S, Harrison SP, Trotta C, & Prentice IC. (2022). Ecosystem Photosynthesis in Land-Surface Models: A First-Principles Approach Incorporating Acclimation. *Journal of Advances in Modeling Earth Systems*, *14*(1), e2021MS002767. https://doi.org/10.1029/2021MS002767

Muir CD. (2019). Is Amphistomy an Adaptation to High Light? Optimality Models of Stomatal Traits along Light Gradients. *Integrative and Comparative Biology*, *59*(3), 571–584. https://doi.org/10.1093/icb/icz085

Murray M, SohWK, Yiotis C, Batke S, Parnell AC, Spicer RA, Lawson T, Caballero R, Wright IJ, Purcell C, & McElwain JC. (2019). Convergence in maximum stomatal conductance of C3 woody angiosperms in natural ecosystems across bioclimatic zones. *Frontiers in Plant Science*, *10*, 558. https://doi.org/10.3389/fpls.2019.00558

Murray M, Soh WK, Yiotis C, Spicer RA, Lawson T, & McElwain JC. (2020). Consistent relationship between field-measured stomatal conductance and theoretical maximum stomatal conductance in C3 woody angiosperms in four major biomes. *International Journal of Plant Sciences*, *181*(1), 142–154. https://doi.org/10.1086/706260

Nick Smith's Ecophysiology Lab, McNellis R, & Keenan T. (2024). *SmithEcophysLab/optimal_vcmax_R: Optimal Vcmax version 3.2.1*. Zenodo. https://doi.org/10.5281/zenodo.14186765

Nimmo V, Violle C, Entz M, Rolhauser AG, & Isaac ME. (2023). Changes in crop trait plasticity with domestication history: Management practices matter. *Ecology and Evolution*, *13*(11), e10690. https://doi.org/10.1002/ece3.10690

Norby RJ, Delucia EH, Gielen B, Calfapietra C, Giardina CP, King JS, Ledford J, Mccarthy HR, Moore DJP, Ceulemans R, De Angelis P, Finzi AC, Karnosky DF, Kubiske ME, … & Oren R. (2005). Forest response to elevated CO_2 is conserved across a broad range of productivity. *Proceedings of the National Academy of Sciences of the United States of America*, *102*(50), 18052–18056. https://doi.org/10.1073/pnas.0509478102

Odé A, Smith NG, Rebel KT, & de Boer HJ. (2025). Temporal constraints on leaf-level trait plasticity for next-generation land surface models. *Annals of Botany*, *136*(2), 263–274. https://doi.org/10.1093/aob/mcaf045

Perkowski EA, Ezekannagha E, & Smith NG. (2025). Nitrogen demand, availability, and acquisition strategy control plant responses to elevated CO_2. *Journal of Experimental Botany*, *76*(10), 2908–2923. https://doi.org/10.1093/jxb/eraf118

Poorter H, Knopf O, Wright IJ, Temme AA, Hogewoning SW, Graf A, Cernusak LA, & Pons TL. (2022). A meta-analysis of responses of C3 plants to atmospheric CO_2: dose–response curves for 85 traits ranging from the molecular to the whole-plant level. *New Phytologist 233*(4), 1560–1596. https://doi.org/10.1111/nph.17802

Poorter H, Niinemets Ü, Poorter L, Wright IJ, & Villar R. (2009). Causes and consequences of variation in leaf mass per area (LMA): A meta-analysis. *New Phytologist* 182(3), 565–588. https://doi.org/10.1111/j.1469-8137.2009.02830.x

Poorter H, Pons TL, & Reichgelt T. (2025). Stomatal Density and Index Are More Responsive to Light Intensity than to [CO_2]: A Meta-Analysis and Implications for Paleo-CO_2 Reconstruction. *Plant Ecophysiology*, *1*, 1. https://doi.org/10.53941/plantecophys.2025.100001

Poorter H, Van Berkel Y, Baxter R, Den Hertog J, Dijkstra P, Gifford RM, Griffin KL, Roumet C, Roy J, & Wong SC. (1997). The effect of elevated CO2 on the chemical composition and construction costs of leaves of 27 C3 species. *Plant, Cell and Environment*, *20*(4), 472–482. https://doi.org/10.1046/j.1365-3040.1997.d01-84.x

Prentice IC, & Cowling SA. (2013). Dynamic Global Vegetation Models. In *Encyclopedia of Biodiversity* (2nd ed., pp. 670–689). Elsevier Inc. https://doi.org/10.1016/B978-0-12-384719-5.00412-3

Prentice IC, Dong N, Gleason SM, Maire V, & Wright IJ. (2014). Balancing the costs of carbon gain and water transport: Testing a new theoretical framework for plant functional ecology. *Ecology Letters*, *17*(1), 82–91. https://doi.org/10.1111/ele.12211

Prentice IC, Liang X, Medlyn BE, & Wang YP. (2015). Reliable, robust and realistic: The three R's of next-generation land-surface modelling. *Atmospheric Chemistry and Physics*, *15*(10), 5987–6005. https://doi.org/10.5194/acp-15-5987-2015

Pritchard SG, Rogers HH, Prior SA, & Peterson CM. (1999). Elevated CO_2 and plant structure: A review. *Global Change Biology, 5*(7), 807–837. https://doi.org/10.1046/j.1365-2486.1999.00268.x

Purcell C, Batke SP, Yiotis C, Caballero R, Soh WK, Murray M, & McElwain JC. (2018). Increasing stomatal conductance in response to rising atmospheric CO_2. *Annals of Botany*, *121*(6), 1137–1149. https://doi.org/10.1093/aob/mcx208

Reich PB. (2014). The world-wide "fast-slow" plant economics spectrum: A traits manifesto. *Journal of Ecology*, *102*(2), 275–301. https://doi.org/10.1111/1365-2745.12211

Sack L, Scoffoni C, John GP, Poorter H, Mason CM, Mendez-Alonzo R, & Donovan LA. (2013). How do leaf veins influence the worldwide leaf economic spectrum? Review and synthesis. *Journal of Experimental Botany, 64*(13), 4053–4080. https://doi.org/10.1093/jxb/ert316

Sage RF, Sharkey TD, & Seemann JR. (1989). Acclimation of Photosynthesis to Elevated CO2 in Five C3 Species1. *Plant Physiology, 89*(2), 590–596. https://academic.oup.com/plphys/article/89/2/590/6083463

Salim M, Chen Y, Ye H, Nguyen HT, Solaiman ZM, & Siddique KHM. (2022). Screening of soybean genotypes based on root morphology and shoot traits using the semi-hydroponic phenotyping platform and rhizobox technique. *Agronomy*, *12*(1), 56. https://doi.org/10.3390/agronomy12010056

Sanchez-Martinez P, Ackerly DD, Martínez-Vilalta J, Mencuccini M, Dexter KG, & Dawson TE. (2024). A framework to study and predict functional trait syndromes using phylogenetic and environmental data. *Methods in Ecology and Evolution*, *15*(4), 666–681. https://doi.org/10.1111/2041-210X.14304

Sanchez-Martinez P, Martínez-Vilalta J, Dexter KG, Segovia RA, & Mencuccini M. (2020). Adaptation and coordinated evolution of plant hydraulic traits. *Ecology Letters, 23*(11), 1599–1610. https://doi.org/10.1111/ele.13584

Schimel D, Stephens BB, & Fisher JB. (2015). Effect of increasing CO_2 on the terrestrial carbon cycle. *Proceedings of the National Academy of Sciences of the United States of America*, *112*(2), 436–441. https://doi.org/10.1073/pnas.1407302112

Schneider CA, Rasband WS, & Eliceiri KW. (2012). NIH Image to ImageJ: 25 years of image analysis. *Nature Methods, 9*(7), 671–675. https://doi.org/10.1038/nmeth.2089

Shao J, Li G, Li Y, & Zhou X. (2022). Intraspecific responses of plant productivity and crop yield to experimental warming: A global synthesis. *Science of the Total Environment*, *840*, 156685. https://doi.org/10.1016/j.scitotenv.2022.156685

Siefert A, Violle C, Chalmandrier L, Albert CH, Taudiere A, Fajardo A, Aarssen LW, Baraloto C, Carlucci MB, Cianciaruso MV, de L Dantas V, de Bello F, Duarte LDS, Fonseca CR, … & Wardle DA. (2015). A global meta-analysis of the relative extent of intraspecific trait variation in plant communities. *Ecology Letters, 18*(12), 1406–1419. https://doi.org/10.1111/ele.12508

Smith NG, & Dukes JS. (2013). Plant respiration and photosynthesis in global-scale models: Incorporating acclimation to temperature and CO_2. *Global Change Biology 19*(1), 45–63. https://doi.org/10.1111/j.1365-2486.2012.02797.x

Smith NG, & Keenan TF. (2020). Mechanisms underlying leaf photosynthetic acclimation to warming and elevated CO2 as inferred from least-cost optimality theory. *Global Change Biology*, *26*(9), 5202–5216. https://doi.org/10.1111/gcb.15212

Smith NG, Keenan TF, Colin Prentice I, Wang H, Wright IJ, Niinemets Ü, Crous KY, Domingues TF, Guerrieri R, Yoko Ishida F, Kattge J, Kruger EL, Maire V, Rogers A, … & Zhou SX. (2019). Global photosynthetic capacity is optimized to the environment. *Ecology Letters, 22*(3), 506–517. https://doi.org/10.1111/ele.13210

Sonawane BV, Sharwood RE, Whitney S, & Ghannoum O. (2018). Shade compromises the photosynthetic efficiency of NADP-ME less than that of PEP-CK and NAD-ME C4 grasses. *Journal of Experimental Botany*, *69*(12), 3053–3068. https://doi.org/10.1093/jxb/ery129

Stocker BD, Wang H, Smith NG, Harrison SP, Keenan TF, Sandoval D, Davis T, & Prentice IC. (2020). P-model v1.0: An optimality-based light use efficiency model for simulating ecosystem gross primary production. *Geoscientific Model Development*, *13*(3), 1545–1581. https://doi.org/10.5194/gmd-13-1545-2020

Taylor SH, Hulme SP, Rees M, Ripley BS, Ian Woodward F, & Osborne CP. (2010). Ecophysiological traits in C3 and C4 grasses: A phylogenetically controlled screening experiment. *New Phytologist*, *185*(3), 780–791. https://doi.org/10.1111/j.1469-8137.2009.03102.x

Tricker PJ, Trewin H, Kull O, Clarkson GJJ, Eensalu E, Tallis MJ, Colella A, Doncaster CP, Sabatti M, & Taylor G. (2005). Stomatal conductance and not stomatal density determines the long-term reduction in leaf transpiration of poplar in elevated CO_2. *Oecologia*, *143*(4), 652–660. https://doi.org/10.1007/s00442-005-0025-4

Von Caemmerer S. (2021). Updating the steady-state model of C4 photosynthesis. *Journal of Experimental Botany* 72(17), 6003–6017. Oxford University Press. https://doi.org/10.1093/jxb/erab266

Wang H, Prentice IC, Keenan TF, Davis TW, Wright IJ, Cornwell WK, Evans BJ, & Peng C. (2017). Towards a universal model for carbon dioxide uptake by plants/704/47/704/158/851 letter. *Nature Plants*, *3*(9), 734–741. https://doi.org/10.1038/s41477-017-0006-8

Wang H, Prentice IC, Wright IJ, Warton DI, Qiao S, Xu X, Zhou J, Kikuzawa K, & Stenseth NChr. (2023). Leaf economics fundamentals explained by optimality principles. *Science Advances*, *9*(3). https://doi.org/10.1126/sciadv.add5667

Wang S, Zhang Y, Ju W, Chen JM, Ciais P, Cescatti A, Sardans J, Janssens IA, Wu M, Berry JA, Campbell E, Fernández-Martínez M, Alkama R, Sitch S, … & Peñuelas J. (2020). Recent global decline of CO_2 fertilization effects on vegetation photosynthesis. *Science*, *370*(6522), 1295–1300. https://doi.org/10.1126/science.abb7772

Wei Z, Abdelhakim LOA, Fang L, Peng X, Liu J, & Liu F. (2022). Elevated CO2 effect on the response of stomatal control and water use efficiency in amaranth and maize plants to progressive drought stress. *Agricultural Water Management*, *266*, 107609. https://doi.org/10.1016/j.agwat.2022.107609

Wong SC, Cowan IR, & Farquhar GD. (1979). Stomatal conductance correlates with photosynthetic capacity. *Nature*, *282*(5737), 424–426. https://doi.org/10.1038/282424a0

Wright IJ, Reich PB, Westoby M, Ackerly DD, Baruch Z, Bongers F, Cavender-Bares J, Chapin T, Cornelissen JHC, Diemer M, Flexas J, Garnier E, Groom PK, Gulias J, … & Villar R. (2004). The worldwide leaf economics spectrum. *Nature*, *428*(6985), 821–827. https://doi.org/10.1038/nature02403

Xie J, Wang Z, & Li Y. (2022). Stomatal opening ratio mediates trait coordinating network adaptation to environmental gradients. *New Phytologist*, *235*(3), 907–922. https://doi.org/10.1111/nph.18189

Xiong D, Douthe C, & Flexas J. (2018). Differential coordination of stomatal conductance, mesophyll conductance, and leaf hydraulic conductance in response to changing light across species. *Plant Cell and Environment*, *41*(2), 436–450. https://doi.org/10.1111/pce.13111

Xu H, Wang H, Prentice IC, Harrison SP, & Wright IJ. (2021a). Coordination of plant hydraulic and photosynthetic traits: confronting optimality theory with field measurements. *New Phytologist*, *232*(3), 1286–1296. https://doi.org/10.1111/nph.17656

Xu H, Wang H, Prentice IC, Harrison SP, & Wright IJ. (2021b). Plant hydraulics coordinated with photosynthetic traits and climate. *bioRxiv*, https://doi.org/10.1101/2021.03.02.433324

Xu Z, Jiang Y, Jia B, & Zhou G. (2016). Elevated-CO_2 response of *stomata and its dependence on environmental factors. Frontiers in Plant Science 7*, 657. https://doi.org/10.3389/fpls.2016.00657

Zheng Y, Li F, Hao L, Yu J, Guo L, Zhou H, Ma C, Zhang X, & Xu M. (2019). Elevated CO_2 concentration induces photosynthetic down-regulation with changes in leaf structure, non-structural carbohydrates and nitrogen content of soybean. *BMC Plant Biology*, *19*(1), 255. https://doi.org/10.1186/s12870-019-1788-9

Zhou J, Cieraad E, & van Bodegom PM. (2022). Global analysis of trait–trait relationships within and between species. *New Phytologist*, *233*(4), 1643–1656. https://doi.org/10.1111/nph.17879